Submarine Magmatic-Hydrothermal Systems at the Monowai Volcanic Centre, Kermadec Arc

MATTHEW I. LEYBOURNE [1]*, ULRICH SCHWARZ-SCHAMPERA [2], CORNEL E. J. DE RONDE [1], EDWARD T. BAKER [2], KEVIN FAURE [1], SHARON L. WALKER [2], DAVID A. BUTTERFIELD [3], JOE RESING [3], JOHN LUPTON [4], MARK D. HANNINGTON [5], GARY J. MASSOTH [1,6], ROBERT W. EMBLEY [4], WILLIAM W. CHADWICK JR. [7], MALCOLM CLARK [8], CHRISTIAN TIMM [1], IAN J. GRAHAM [1], IAN C. WRIGHT [9]

[1]*GNS Science, P.O. Box 30-368, Lower Hutt, New Zealand*

[2]*Bundesanstalt für Geowissenschaften und Rohstoffe, Stilleweg 2, 30655 Hannover, Germany*

[2]*Pacific Marine Environmental Laboratory, National Oceanic and Atmospheric Administration, 7600 Sand Point Way, Seattle, Washington 98115-6349, U.S.A.*

[3]*JISAO, University of Washington, 7600 Sand Point Way NE, Seattle, WA 98115-6349, United States*

[4] *Pacific Marine Environmental Laboratory, National Oceanic and Atmospheric Administration, 2115 S.E. OSU Drive, Newport, Oregon 97365-5258, USA*

[5] *Department of Earth Sciences, University of Ottawa, Ottawa, Ontario K1A 0E8, Canada*

[6] *Mass-Ex3 Consulting LLC, 2100 Lake Washington Boulevard N, Renton, WA 98056, United States*

[7] *Hatfield Marine Science Center, Oregon State University, Newport, Oregon, USA.*

[8] *National Institute of Water and Atmosphere, Greta Point, Wellington, New Zealand*

[9] *National Oceanography Centre, Southampton, University of Southampton Waterfront Campus, European Way, Southampton SO14 3ZH, United Kingdom*

* Corresponding author; m.leybourne@gns.cri.nz

For submission to Special Issue of Economic Geology

Abstract

The Monowai volcanic centre (MVC) is located at the mid-point along the ~2530 km long Tonga-Kermadec arc system, is probably the most hydrothermally active submarine volcanic system globally. The MVC is comprised of a large elongate caldera (Monowai caldera, 7.9 x 5.7 km; 35 km^2; depth to caldera floor is 1590 m), which has formed within an older caldera some 84 km^2 in area. To the south of the nested caldera system is a large composite volcano, Monowai cone, which rises to within ~ 100 m of the sea surface and has been volcanically active for at least several decades. Despite the large size, mafic volcanic rocks dominate the MVC; basalts are the most common rock type recovered; less common are basaltic andesites and andesites. Hydrothermal plume mapping during the 2004 NZAPLUME III cruise showed at least three major hydrothermal systems associated with the caldera and cone. Monowai cone has hydrothermal venting from the summit. This summit plume is gas-rich and acidic; plume samples show a pH shift of -2.00 pH units, δ^3He up to 358 ‰, H_2S concentrations up to 32 μM and CH_4 concentrations up to 900 nM. The summit plume is also metal-rich with elevated total dissolvable Fe (TDFe up to 4200 nM), TDMn (up to 412 nM), and TDFe/TDMn (up to 20.4). Monowai caldera has a major hydrothermal vent system with plumes extending from ~ 1000 to 1400 m depth. The caldera plume has lower values for TDFe, although ranges to higher TDMn concentrations than the summit plume, and is relatively gas-poor (no H_2S detected, pH shift of -0.06 pH units, CH_4 concentrations up to 26 nM). Hydrothermal vents have been observed associated with prominent basaltic-andesite ridges (Mussel Ridge) proximal to the southwest wall of the caldera (1025 – 1171 m depth). However, the composition of the hydrothermal plumes in the caldera are different to the vents, indicating that the source of the caldera plumes is at greater depth and is more metal-rich and therefore likely higher temperature. Minor plumes detected as light scattering

anomalies down the northern flank of Monowai caldera most likely represent resuspension of volcanic debris.

Particulate samples from both the cone sites and the caldera site are enriched in Al, Ti, Ca, Mg, Si, and S, with the cone summit plume especially enriched in K, As, W and Cu, Pb, Zn. The elevated Ti and Al suggest acidic water-rock reactions and intense high-sulfidation alteration of the host volcanic rocks. Observations from submersible dives with *Pisces V* in 2005 and the remotely operated vehicle *ROPOS* in 2007 of Mussel Ridge indicate numerous low temperature vents (< 60°C), with a large biomass of vent-associated fauna, in particular large accumulations of the mussel *Bathymodiolus* sp. and the tubeworm *Lamellibrachia* sp.

We interpret the Monowai volcanic centre as possessing a robust high-sulfidation magmatic-hydrothermal system, with significant differences in the style and composition of venting at the cone and caldera sites. At Monowai cone, the large shifts in pH, elevated TDFe and TDFe/TDMn, and H_2S-, CH_4- and ^3He-rich nature of the plume fluids coupled with elevated Ti, P, V, S and Al in the particulates indicates significant magmatic volatile ± metal contributions to the hydrothermal system and aggressive acidic water-rock interaction. By contrast, Monowai caldera has low TDFe/TDMn in hydrothermal plumes; however, end-member vent fluid compositions, combined with presence of alunite, sulfide minerals and native sulfur in samples from Mussel Ridge suggest recent acid volatile-rich venting and active Fe-sulfide formation in the subsurface, and the potential for the presence of significant SMS mineralization.

Introduction

Hydrothermal systems have long been studied on mid-ocean ridges (MOR) to better understand heat-flow and chemical fluxes to the oceans from oceanic crust and the upper mantle. The contribution of hydrothermal systems associated with submarine volcanic arcs has only begun to receive attention in the last ten years (de Ronde et al., 2001; Baker et al., 2008; de Ronde et al., 2009). As part of this effort to understand arc volcanism and hydrothermal processes, the Kermadec arc northeast of New Zealand has been systematically surveyed for evidence of hydrothermal activity (de Ronde et al., 2001; Baker et al., 2003; de Ronde et al., 2007). Although these surveys have documented that ~ 70% of the submarine volcanic centres along the Kermadec arc are presently hydrothermally active, to date only one of these centres, Brothers volcano, has been the focus of detailed study. Brothers volcano is host to at least two major hydrothermal systems, the NW caldera site, which is characterized by high temperature (~ 300°C), focussed black smoker venting, Cu-Au-rich massive sulfide mineralization, and the cone site, which has lower temperature (< 130°C), diffuse gas-rich acidic vent fluids (de Ronde et al., 2005; de Ronde et al., 2011, in press). These hydrothermal systems at Brothers provide clear evidence for direct magmatic contributions to the hydrothermal fluids, and are thus similar to systems on several subaerial volcanic islands along the Kermadec arc, including White Island, Raoul Island and Curtis Island. Brothers volcano is situated relatively close to the NZ subcontinent and, as such, is potentially influenced by subduction of continentally derived sediments and the Hikurangi plateau (Fig. 1) (de Ronde et al., 2007). Curtis and Raoul volcanic centres are located on top of the Kermadec Ridge and so are associated with thicker arc crust than systems in the southern and northern parts of the Kermadec arc (Fig. 1b). The Monowai Volcanic Centre (MVC), located mid-way along the ~2530 km long Kermadec-Tonga arc/backarc system, sits west of the Kermadec Ridge by ~ 35 km and is the most distal volcanic centre from influence

of subduction of sediment derived either from New Zealand or the Tongan Islands. Monowai is characterized by a large caldera (~ 35 km^2; Monowai caldera) and a large cone (Monowai cone) to the south of the caldera, and is dominated by mafic volcanic rocks. Monowai caldera is thus atypical of large oceanic and continental calderas, which are typically dominated by silicic rocks. The setting (far from continental influence) and rock chemistry (mafic) therefore provides an excellent opportunity to study the hydrothermal chemistry of an arc hydrothermal system that is in significant contrast to the well-studied Brothers volcano. Monowai cone, which comes to within < 150 m of the sea surface, has been volcanically active for at least several decades (Davey, 1980), and low temperature diffuse venting was discovered there in 1998 during the SO-135 cruise by the R/V Sonne (Stoffers et al., 1999). Monowai has been revisited by several research cruises, including NZAPLUME III (New Zealand American PLUme Mapping Expedition) in 2004, the NZASRoF (New Zealand American Submarine Ring of Fire) in 2005 and the MANGO cruise in 2007 (Schwarz-Schampera et al., 2007). In contrast to the cone, Monowai caldera was only recently discovered, by swath mapping during the NZAPLUME III cruise.

The study of submarine arc hydrothermal systems is important, not only to better understand heat and chemical fluxes to the oceans, but also in terms of ore-deposit forming processes. Although massive sulfide mineralization has been studied on MORs for decades, as analogs to ancient on-land volcanogenic massive sulfide deposits, it is likely that arc volcanoes provide much better analogs because they are more likely to be preserved than MOR, which typically are subducted. The nature of arc volcanism is such that magmatic and therefore hydrothermal systems are likely to be much longer-lived, producing larger deposits, than at MORs, where seafloor spreading occurs. Furthermore, there is controversy over the extent to which direct magmatic inputs contribute to volatile and metal loads of seafloor massive sulfide (SMS) mineralization for MORs, whereas the greater depth range and

generally shallower nature of arc hydrothermal systems provides us better insights into how magmatic fluids contribute to seafloor hydrothermal systems (e.g., Stanton, 1991; Hannington et al., 1995; Yang and Scott, 2002; Beaudoin and Scott, 2009).

This paper presents a synthesis of the current understanding of a large submarine arc volcanic centre and its hydrothermal systems, based on hydrothermal plumes and vent fluids, bathymetric mapping, submersible observations, and recovered rock and mineralised samples. Here, we seek to characterize the system, determine the extent to which magmatic volatiles influence the chemistry of the vent fluids and the resultant hydrothermal plumes, and determine the potential for SMS mineralization in the subsurface. This study provides an important contrast with Brothers volcano in the southern Kermadec arc, because although both systems are dominated by large calderas and active hydrothermal vents, Brothers caldera is silicic and has high temperature vents (~ 300 °C) with known SMS mineralization, whereas Monowai is a predominantly mafic caldera and cone system, has no obvious SMS deposits, and only relatively low temperature (< 60 °C) venting has been observed to date.

The Tonga-Kermadec Arc

The Kermadec arc represents the southern portion of the ~2,500 km long Kermadec-Tonga arc, formed by the subduction of the Pacific Plate westwards underneath the Australia Plate (Fig. 1). Although there are about 57 submarine volcanic centers along the entire arc, most (33) occur along the 1,220 km-long part of the Kermadec arc (de Ronde et al., 2005). The southern portion of the active Kermadec arc front (south of ~ 32°S) is represented by submarine stratovolcanoes that occur west of the high-standing Kermadec Ridge (Fig. 1) (Wright et al., 1996). The southward transition from oceanic to continental crust, combined with subduction of continentally-derived sediments and overthickened oceanic crust of the Hikurangi Plateau, results in a variety of magma source compositions that are reflected in the

elemental and isotopic composition of erupted products along the arc, and likely reflects in the variability in the hydrothermal fluids, mineralization styles, and intensity of venting (de Ronde et al., 2001; Massoth et al., 2003; de Ronde et al., 2005; de Ronde et al., 2007).

The backarc to the Kermadec-Tonga volcanic arc comprises the Lau-Havre-Taupo backarc complex (Fig. 1), which is southward propagating and undergoing active extension. This backarc complex evolves from north to south as oceanic spreading in the central and northern Lau Basin, through rifting of arc crust along the southernmost Lau Basin and the Havre Trough, and includes continental rifting within New Zealand (Wright et al., 1996). West of the Lau Basin and Havre Trough is the Colville Ridge, a remnant arc, which became isolated from active arc volcanism at ~ 5.5 Ma. The Lau Basin undergoes more rapid extension compared to the Havre Trough, with rates as high as 159 mm yr^{-1} in the northern Lau Basin, whereas extension is 15-20 mm yr^{-1} in the Havre Trough. The transition from more rapid extension and oceanic spreading in the Lau Basin to rifting-dominated extension in the Havre Trough occurs where the trench-oblique Louisville Seamount Chain is subducted; subduction of this chain has progressively migrated southwards over the last 4 Ma (Wright et al., 1996).

Monowai volcanic centre

Volcanic rocks have been recovered from Monowai caldera and cone, as well as several smaller satellite cones (Fig. 2). Samples were recovered by dredging during SO-135 and NZAPLUME III (Haase et al., 2002; Graham et al., 2008), in addition to dives by *Pisces V* and *ROPOS* (Embley et al., 2006; Schwarz-Schampera et al., 2007). Graham et al. (2008) defined two caldera structures at Monowai, including a larger older caldera in which the younger deeper and hydrothermally active caldera has formed; whether these calderas represent two discrete caldera-forming events or one continuous event is, in the absence of

good age control on the volcanic rocks, unknown at this stage. To the south of Monowai caldera, recent volcanic activity is centred at Monowai cone, a large stratovolcano. There are also a number of parasitic cones around the rim of the caldera and a small cone, possibly a resurgent dome, in the centre of Monowai caldera (Fig. 2). The active caldera is elongated NW-SE (as is Brothers volcano in the southern Kermadec arc; de Ronde et al., 2005); the entire volcanic centre also appears to be similarly elongated (Graham et al., 2008). Proximal to the SW wall of Monowai caldera there are two subparallel ridges, including Mussel Ridge, where caldera hydrothermal activity is presently focussed (Fig. 3). The parasitic cones are clearly disrupted by faulting (Fig. 2), and predate the main cone and most recent caldera (Graham et al., 2008). The older caldera has the largest volume of any caldera in the northern section of the Kermadec arc. The main cone has a constructional volume between 11 and 14 km^3 (Graham et al., 2008). Repeat bathymetric mapping of the Monowai cone (e.g., 1998, 2004, 2007) demonstrates that it is highly dynamic with repeated construction and sector collapse (Chadwick et al., 2008; Wright et al., 2008). Monowai cone has been erupting for at least the last several decades.

The majority of rocks collected from Monowai are basaltic in composition, with less common basaltic andesites and andesites. If Monowai is truly dominated by basalts, it is then a relatively large mafic caldera by global standards. Graham et al. (2008) described the major element and mineralogical characteristics of the rocks collected from the Monowai volcanic centre during NZAPLUME III and noted that samples from Monowai cone are entirely basaltic with weighted mean SiO_2 contents of 50% compared to the calderas, where recovered samples are basaltic to basaltic-andesite to andesite with weighted mean SiO_2 contents of around 55%. For greater details on the geochemistry of the rocks at MVC, see Timm et al. (2011 in press).

Methods

Samples were collected during the 2004 NZAPLUME III cruise on the R/V *Tangaroa,* the 2005 *Pisces V* cruise on the R/V *Ka`imikai-o-Kanaloa*, and the 2007 MANGO 192-2 *ROPOS* cruise on the R/V *Sonne*. Vertical casts and tow-yos were carried out over both the Monowai caldera and Monowai cone (Fig. 2). Full details of sampling and analytical methods are presented in the electronic annex (EA1).

Results

Hydrothermal plumes

Conductivity-Temperature-Depth-Optical (CTDO) results: The MVC hosts the most extensive hydrothermal system found in the northern segment of the Kermadec arc (i.e., during NZPLUME III; Fig. 1B). A series of five CTDO tow-yos and seven vertical casts were conducted across the caldera and cone structures (Fig. 2). In the caldera, large-scale diffuse venting sources are located along the easternmost (inner) of a series of ridges forming the western wall of the caldera (Fig. 3, 4). These hydrothermal vents form a series of plumes that filled the western and northern portions of the 500-m-deep caldera (Fig. 5). There is no apparent hydrothermal activity associated with the resurgent cone in the centre of the caldera. South of the caldera, abundant hydrothermal sources were found on the 1000-m-high Monowai volcanic cone. Plumes were found at the summit (~130 m depth) and associated with small satellite cones at ~400 and ~600 m on the northern flank (Fig. 5D). Venting at the summit was particularly intense, commonly reaching maximum LSS NTU levels (5.0; Table 1) on vertical casts over the summit. Weak venting may occur on a smaller cone to the northwest, with LSS anomalies at ~ 800 depth, seen in T04A-08 (Fig. 5C), although this plume may also represent spill over from the caldera.

pH and H_2S: Hydrothermal plumes associated with both Monowai cone and caldera display different chemical compositions based on discrete samples collected by vertical casts and tow-yos (Figs. 6, 7). Plumes above the cone summit site have some of the largest shifts in pH recorded along the Kermadec arc, with shifts up to -2.00 pH units relative to background seawater (Fig. 6A). Plume samples with the largest shifts in pH also have the highest ΔNTU values (Fig. 6) and TDFe concentrations (Fig. 7A). Hydrothermal plumes within Monowai caldera have shifts of up to -0.06 pH units over background (Fig. 6B). Although the caldera plume has a smaller pH shift than the cone summit plume, shifts of this magnitude are common on hydrothermally active volcanoes along the mid-Kermadec arc, but lower than most of those on the southern-Kermadec arc (de Ronde et al., 2001; de Ronde et al., 2007). The lowest pH by direct measurements of hydrothermal vent fluids within the caldera during *Pisces V* dives was 5.4 (see below). These caldera vent pH values in turn imply that the vents at the cone summit, which have not been directly sampled, are likely considerably lower in pH at the vent source(s).

Hydrogen sulfide was only detected in plume samples over Monowai cone, with concentrations ranging from less than detection (~ 1 μM) up to 32 μM. The highest H_2S concentrations are in excess of those recorded for the most hydrothermally active volcano along the Kermadec arc, Brothers volcano, where H_2S concentrations in plumes samples are < 10 μM (de Ronde et al., 2005). Although plume samples from Monowai caldera were all below detection, vent fluids collected using *Pisces V* from the vent field in the caldera have elevated H_2S concentrations (see below).

Total dissolvable Fe and Mn: Monowai cone hydrothermal plume samples have elevated total dissolvable metal concentrations, coincident with the largest pH and H_2S anomalies (Fig. 7). TDFe and pH co-vary (Fig. 7A). However, there appears to be a threshold value of ~

1000 nM TDFe where pH decreases rapidly with only relatively small increases in TDFe. There is a positive correlation between TDFe and particulate (PFe) concentrations, expressed as a power law function where $PFe = 5.03 \cdot TDFe^{0.66}$ (Fig. 7B). The summit plume of Monowai cone is characterized by elevated TDMn concentrations (Fig. 7C, 8B). Here, TDMn concentrations are as high as 412 nM. By contrast, the caldera plume has the highest TDMn concentrations, ranging up to 775 nM (Fig. 7C).

For the whole data set for Monowai, TDFe concentrations increase from background concentrations to ~ 100 nM TDFe with little change in TDMn concentrations, at which point TDMn rapidly increases with little change in TDFe, which likely reflects oxidation of Fe^{2+} and precipitation of Fe^{3+} oxyhydroxides in the plume and scavenging of both hydrothermal Mn and seawater (hydrogenous) Mn. Most of the plume samples from the caldera and cone are elevated in TDFe (with respect to seawater values), so that even though the particulate Fe and base metal contents for the caldera are not highly elevated (see below), the Fe is clearly anomalous and reflects extensive and robust hydrothermal venting. There is a strong positive correlation between DFe and TDFe; however, the ratio DFe/TDFe increases with decreasing TDFe concentration (for TDFe > 500 nM, DFe = 40 to 81% TDFe, whereas for TDFe < 500 nM, DFe = < 5 to 41% TDFe), implying that at the highest Fe concentrations, most of the Fe occurs either as Fe^{2+} and/or is present as fine colloids that pass through the 0.4 μm filter.

Depth profiles for TDFe and TDMn demonstrate that the plumes have different chemical characteristics (Fig. 8A and 8B). Elevated TDFe and TDMn concentrations characterize the summit plume, whereas the caldera plume has higher TDMn concentrations relative to the TDFe. The deeper plume on the cone is characterized by elevated TDFe values, but background TDMn values. As a result, TDFe/TDMn values for the summit plume are higher than for the caldera. By comparison, plumes at 600 and 800 m depth on the north flank of the cone have the highest TDFe/TDMn values, in excess of 20 (Fig. 8D). Although the plume at

~450 m is clearly visible in the LSS data (Fig. 5), this plume has no associated anomaly in TDMn and subtle increases in TDFe, at best (Fig. 8). This plume at around 450 m depth is most likely not hydrothermal in origin, but is more likely a turbidity-type plume (e.g., Walker et al., 2008). By contrast, DMn is in all cases > 40% of TDMn, with most samples with > 100 nM TDMn having essentially 100% of the Mn in "dissolved" form.

Methane and helium: Methane (CH_4) concentrations for the cone summit plume are elevated, ranging up to 895 nM (Table 1; Fig. 9). Although there are LSS anomalies at around 450 m on the cone, there are no coincident CH_4 anomalies (Fig. 9). By contrast, the LSS anomaly at ~ 600 m depth on Monowai cone has CH_4 concentrations up to 15 nM, significantly above background for this depth of ~ ≤ 2 nM. Samples from the caldera are also elevated in CH_4 over regional background, reaching a maximum of 26 nM (Fig. 9A). With the exception of the summit plume at the cone site, there is an inverse relationship between CH_4 and TDFe/TDMn (Fig. 9B), as well as between TDFe concentrations and CH_4/TDMn (not shown).

At Monowai cone and caldera δ^3He values range up to 358 %, with the most elevated values associated with the cone summit plume (Fig. 9C; see EA1 for definition of δ^3He). These elevated δ^3He values are the highest along the Kermadec arc; δ^3He values > 300 % have also been recorded at the volcanically and hydrothermally NW Rota-1 volcano on the Mariana arc (e.g., Resing et al., 2007; Lupton et al., 2008) and W. Mata (J. Lupton, unpublished data). Within the Monowai caldera hydrothermal plume, samples with elevated LSS values have δ^3He values between 15 and 28%, well above background values of < 10 % δ^3He for samples with low LSS (Table 1; Fig. 9). Regressing ^{3}He against ^{4}He permits the determination of the R/R_A-value, where R_A is the $^3He/^4He$ ratio in air. Monowai cone summit plume samples define a tight linear trend with R = 9.6 (r = 1.00), yielding an R/R_A of 6.7.

This R/R_A value is similar to that recorded for other volcanoes along the Kermadec arc (e.g., de Ronde et al., 2007). The plumes along the flanks of Monowai cone are not anomalous with respect to ^3He (Fig. 9C).

Particulate Chemistry

Particulates were analyzed for samples with elevated ΔNTU values from both the caldera and cone tow-yos and casts (Table 2). Cone samples come from depths < 810 m, whereas caldera samples are all > 1000 m (Table 2). There are some key differences between the two sets of samples. Cone samples commonly have elevated Ti concentrations, ranging up to 74 mM, whereas caldera samples are all < 7 mM. These Ti concentrations are higher than most volcanoes along the Kermadec arc and higher than plumes along the MORs (de Ronde et al., unpublished data, Baker et al., 2003). Total S concentrations are variable for both the cone site and the caldera, but for the cone range to values up to 20,000 nM. Highest total S concentrations for the caldera are more than an order of magnitude lower (Table 2). The speciation of S in the particulate samples from Monowai is variable, ranging from essentially 0 to 100% of the total S as volatile S, with increasing % volatile S as total S concentrations increase. Particulate Fe concentrations are variable, ranging from 2 to 2600 nM at the cone and from 70 to 160 nM at the caldera. By contrast, particulate Mn is less variable with all samples ranging from 0.1 to 8 nM. Monowai particulates have relatively low Cu, Zn and Pb concentrations with maximum concentrations of 2.3, 3.9, and 0.4 nM, respectively.

Pisces V observations

A total of four dives were carried out at the caldera vent site using *Pisces V* during the NZARoF Cruise (Embley et al., 2006) (Fig. 3). Dive PV-612 began on the floor of Monowai caldera near a SW-NE trending tectonic ridge extending from the resurgent cone of the

caldera floor into the SW wall of the caldera. The submersible traversed upslope towards Mussel Ridge and passed over alternating areas of pillow lavas, heavily sedimented areas and talus slopes (Fig. 3). At about 1200 m depth, dense communities of small bivalves and limpets colonized unsedimented pillow flows. Swarms of shrimp were observed on the ledges of outcrops and at 1056 m dense mussel beds and swarms of crabs and shrimp were observed. The mussel beds (Fig. 4F) were mapped for more than 300 meters along the crest of the ridge to the southeast. In places the mussels almost completely covered the seafloor. The crab population was large. The fauna are indicative of local diffuse hydrothermal venting.

Dive PV-613 started on the lower southeastern flanks of Mussel Ridge, which was dominated by pillow lavas and associated talus (Fig. 3). The western flanks of the ridge comprised a similar geology on the lower slopes. The upper slopes consisted of volcanic talus and mussel shell detritus. The northeastern flank comprises a NE-SW structurally controlled hydrothermal vent field, extending from a depth of 1170 m to the ridge crest. The field consists of discrete vents with associated mussels beds, crabs, shrimps, and tubeworms (Fig. 4C-F). Most vents occur at outcrop bases with evidence of elemental sulphur extrusion on the seafloor (Fig. 4C, D). Vent temperatures ranged between 47°C and 55°C. Dive PV-614 was focused mainly on collection of vent fluids for chemical analysis. Dive PV-615 explored a small cone located NW of Mussel Ridge and another distinct biological community on the southern flank of the cone was observed. Sulfur crusts, low temperature venting and Fe-staining were common.

In summary, *Pisces V* dives showed that the Monowai caldera vent site on Mussel Ridge is dominated by pillow and pillow tubes flows of basalt to basaltic-andesite, commonly sedimented and rippled, with numerous talus piles and scarps. Low temperature venting (< 60°C) is commonplace, consistent with the area surveyed having a high biomass dominated by hydrothermal vent-associated species.

Hydrothermal alteration at Mussel Ridge

Samples of hydrothermally altered rock were collected during the Mango 192-2 cruise using the remotely operated vehicle *ROPOS*. Sampling revealed extensive hydrothermal alteration of the mafic host rocks and disseminated sulfide mineralization. Hydrothermal venting was observed at Mussel Ridge, which represents a volcanic ridge at the lower part of the Monowai caldera wall. Volcanic rocks are represented by (micro-)vesicular, aphyric, glassy basaltic to andesitic lava and partly oxidized volcaniclastic sediment. Strong alteration is particularly pronounced along cracks and fissures within the rocks. Amorphous silica, fine-grained cristobalite, natroalunite and natrojarosite are intergrown with pyrite and marcasite (Fig. 10). Traces of magnetite and chalcopyrite, as well as anhydrite, barite, pyrophyllite and smectite are also present. Native sulfur occurs as cement for brecciated lapilli ash particles. In strongly altered samples, the mineralogy is completely replaced by silica-alunite-pyrite(±pyrophyllite) assemblages (acid sulfate-type) or relict silica phases, which remain after breakdown of rock forming minerals (vuggy silica-type). Although sampled fluids at Mussel Ridge show low temperature and near-neutral pH characteristics, there is strong mineralogical evidence that higher temperature, acid sulfate fluids are responsible for the prevailing alteration characteristics (Schwarz-Schampera et al., 2007; Schwarz-Schampera et al., 2008).

The composition of texturally well-preserved glass fragments, weakly altered basalts and basaltic andesites, strongly altered and mineralized basaltic andesites, alteration crusts and massive precipitates of native sulphur was determined (Fig. 11; Table 3). Compared to fresh volcanic glass, distinctly representing basaltic andesitic composition for most of Mussel Ridge, it is evident that the alkalis, silica, iron, and magnesium, as well as large amounts of the low field strength elements (Ba, Rb, Sr, Cs) have been mobile. The alteration silica-

alunite-pyrite(±pyrophyllite) assemblage and relict phases remaining after breakdown of rock forming minerals results in high Na_2O and SiO_2 contents of the altered samples, respectively. Other major elements and the high field strength elements (Ti, Zr, Hf, Nb, Ta, Y, P) can be considered immobile during the alteration process. Alteration process has led to slight enrichments in Cu (up to 261 ppm), As (up to 22 ppm), Sb (up to 12 ppm), Ba (up to 340 ppm), and Au (95 ppb) in sulphide-bearing rocks (Fig. 11; Table 3).

The range of isotopic compositions of the sulphide (pyrite), sulfate (alunite) and native sulphur is typical of volcanic-derived sulfur in seafloor hydrothermal systems likely reflecting variable contributions from reduced seawater sulfate and a deeper magmatic source. $\delta^{34}S$ values of the pyrite separates are uniformly at -8.4 ‰ (Table 4). Alunite samples (n = 5) have $\delta^{34}S$ values ranging from 1.2 to 11.3 ‰, distinctly lower than seawater sulfate. The $\delta^{34}S$ values of the native sulfur separate samples range from 1.2 to 2.8 ‰ (Table 4). Applying the sulfate (alunite) – sulfide (pyrite) geothermometer of Ohmoto and Lasaga (1982) to the widest range in $\delta^{34}S$ values for alunite (+7.9 ‰) and pyrite (-8.5 ‰) yields a temperature of formation of around 300°C; unrealistically high temperatures are derived using the isotopically lighter alunite (> 500°C).

Vent fluid chemistry

Vent fluids from Monowai caldera were collected during the *Pisces* V cruise in 2005 within an area less than 1x1 km near a ridge on the west side of the caldera near 25° 48’ S and 177° 10’ W (mark on the map showing CTD tow tracks). Several different vents were sampled at depths between 1170 and 1050 m. No attempts have been made to sample vent fluids from Monowai cone owing to its on-going volcanic activity. No high temperature vents were observed during the *Pisces* V and *ROPOS* dives in Monowai caldera. Maximum vent

fluid temperatures were 57°C in 2005 and 42°C in 2007. No fluid chemistry from 2007 is presented here.

The vent fluids at Monowai caldera have high Mg concentrations ranging from 48.0 to 52.1 mmol/kg (92 to >99% of measured ambient seawater Mg, 52.33). We will examine the measured fluid properties before considering the properties of a putative zero-Mg end member fluid. For fluid samples with temperature > 10°C, the pH is between 5.3 and 5.9, and none of the fluids have sulphate concentrations higher than ambient seawater. Hydrogen sulphide is highly enriched for low-temperature fluids, with measured concentrations up to 4 mmol/kg and H_2S/heat ratios near 20 nmol/J. Many of the fluids have a measured excess of total dissolved sulphur (H_2S + SO_4) relative to ambient seawater. Dissolved silica is also enriched up to 1490 µmol/kg (local background seawater is 57 µmol/kg). Several different vent sites were sampled and two of those sites yielded samples with low chlorinity. An additional five sites had chlorinity very close to seawater values (Table 5). Major cations show evidence of water/rock reaction. Mg is lower than seawater in all samples, and the measured Mg/Cl ratio is as low as 95% of the measured seawater ratio. Sodium and potassium are also depleted, with Na/Cl and K/Cl ratios as low as 84% of the seawater ratio in one sample. Calcium is enriched above seawater in all vent samples, with Ca/Cl ratios up to 122% of the measured seawater ratio.

Trace elements are enriched in Monowai vent fluids from water/rock reaction. Iron concentrations are low, ranging from 0.3 to 5.2 µmol/kg with one anomalous sample at 70 µmol/kg. Manganese concentrations range from 25 to 417µmol/kg, and Fe/Mn ratios are generally near 0.01, with two values near 0.2. The low Fe/Mn ratios are typical of diffuse fluids and are indicative of loss of iron below the seafloor (e.g. Butterfield and Massoth 1994). Cesium is enriched up to 4 times above ambient seawater concentration.

The vent fluids are moderately gas-rich with measured concentrations of ^{3}He (0.37 to 1.68 pmol/kg), CO_2 (6.4 to 9.5 mmol/kg), and CH_4 (21.5 to 38.7 µmol/kg) (Fig. 12) close to or exceeding those from Brothers volcano (de Ronde et al., 2011, in press).

The near-linear trends of Si, H_2S, and SO_4 with Mg suggest that there may be a zero-Mg fluid at depth, although no vent fluids sampled at Monowai caldera have Mg concentrations close to zero as would be expected for an *undiluted* hydrothermal end-member produced by approach to equilibrium between fluid and rock at high temperature (Edmond et al., 1979; Seyfried, 1987). When plotted versus Mg, there is significant scatter in all of the other measured components, so conservative mixing of a single high-temperature end member does not explain the data. The low-chlorinity fluids form a separate trend from the remaining near-seawater chlorinity fluids.

Using different geothermometers for quartz yields a temperature of around 320-350°C for the last equilibration of the end-member fluid (Verma, 2008). Because of the extent of subsurface seawater mixing, these Si geothermometer results should be treated with caution. However, although there is scatter in the Si versus Mg for the vent fluids (Fig. 12), these temperature estimates are broadly similar to that derived from nearby mineral samples for the pyrite-alunite $\delta^{34}S$ geothermometer of at least 300°C. Given the uncertainties in estimates of end-member Na, K (Fig. 12) and Li concentrations, geothermometers based on the alkali metals do not yield meaningful results.

Vent fauna at Mussel Ridge

The biological samples collected from Monowai caldera are still being examined by taxonomists in several institutes. On account of sampling along the Kermadec arc expanding in recent years, care is needed to distinguish geographical variation from definite speciation. With many vent taxa, this requires molecular as well as morphological techniques, and

numerous samples. Nevertheless, the photographic data from *ROPOS* and *Pisces V* dives, coupled with direct samples, enable a provisional description of some key elements of the Monowai caldera vent system. Clumps of the tubeworm *Lamellibrachia juni* (Fig. 4E) were common, but not dense. A number of the clumps comprised small-sized worms, suggesting they were relatively young. The bathymodiolid mussels (*Bathymodiolus ?brevior*) (Fig. 4F), conversely, formed dense patches, extending hundreds of metres in horizontal extent along 'Mussel Ridge". The mussel beds were commonly covered in lithodid crabs, *Paralomis hirtella*. These crabs are scavengers, but clearly able to tolerate elevated temperature and sulphide levels in the water and their prey. The other notable taxa were alvinocarid shrimps, *Alvinocaris niwa* and *Alvinocaris longirostris*, which were in places observed in high densities.

Discussion

Plume fluids and particulates

There are three different plume types evident from the CTDO tow-yos and casts (Fig. 5). These are: 1) the Monowai cone summit plume, which is gas-rich, has a large pH shift (larger than any pH shift observed to date on the Kermadec arc) and is Fe-rich; 2) the Monowai caldera plume, which is characterized by a relatively small pH anomaly but has the largest TDMn anomaly together with elevated LSS and CH_4; and 3) several plumes (~ 450, 600, and 800 m depth on the north flank of Monowai cone), which have variable LSS, CH_4 and TDFe anomalies, but no pH or Mn anomalies, and most critically, no He anomalies. The LSS plumes down the flank of Monowai cone are probably not hydrothermal and most likely reflect resuspension of mafic pyroclasts during eruption and/or mass wasting, as has been observed at NW Rota-1 on the Mariana arc (Walker et al., 2008; Walker et al., 2010).

Iron and Mn concentrations vary as a function of plume height above the vent source sampled, lateral distance from the source, and the age of the plume (signal attenuation by oxidation of hydrothermal Fe^{2+} and seawater dilution). Whereas Fe is oxidized rapidly (minutes to hours, Statham et al., 2005), Mn oxidation occurs over significantly longer time frames, i.e., months to a year or more (Cowen et al., 1990; Kadko et al., 1990). The rate of Fe oxidation is in part controlled by ambient pH and dissolved oxygen concentration, with recent experimental work on active vent sites showing that microbial interaction may also influence oxidation rates (Statham et al., 2005; Bennett et al., 2008). Assuming a hydrothermal vent fluid Fe concentration of 1 mM, a plume with TDFe = 4000 nM would have undergone 250x dilution; this Fe concentration (and therefore calculated dilution) is a minimum as vent fluids at NW Rota-1 commonly have TDFe > 1 mM (Butterfield et al., in press). A shift in pH of -2.00 pH units implies that the original vent fluids were very acidic, similar to or more acidic than those at the cone site at Brothers volcano (de Ronde et al., 2005) and NW Rota 1 on the Mariana arc (Resing et al., 2007). The pH shift for the Monowai cone summit plume is significantly greater than that at Brothers cone (-0.44 pH units) and NW Rota 1 (-0.73 pH units), implying that the plume samples at Monowai were either sampled closer to the source (i.e., less dilution by ambient seawater) or that the vent fluids are more CO_2, SO_2 and H_2S-rich at Monowai cone. The greater magnitude of the pH, and H_2S plume anomalies for the Monowai cone plume compared to Brothers cone plume with both having similar TDFe concentrations, is consistent with less dilution and a highly acidic (SO_2-rich) source fluid at Monowai cone.

Hydrothermal vent fluids associated with arc volcanoes commonly have elevated Fe/Mn values compared to vent fluids along MORs (Massoth et al., 2003). For example, whereas MORs typically have Fe/Mn values around 2-4, arc volcanoes commonly have Fe/Mn significantly higher (e.g., Brothers volcano at 18.2). Fluids from an active volcanic vent at

NW Rota-1 have Fe/Mn up to 55, identical to the source rock and attributed to rapid dissolution of fresh volcanic rock by SO_2-rich magmatic fluids (Butterfield et al in press). At Monowai volcano, the different hydrothermal systems have different Fe/Mn values (Fig. 7). The caldera plumes have variable TDFe/TDMn values, ranging from < 1 to ~ 52; these plumes have generally elevated Mn relative to CH_4 concentrations and change in pH compared to the cone plumes (e.g., Fig. 7C, 8B). Note however, that the vent fluids sampled at Mussel Ridge all have TDFe/TDMn < 1, with most < 0.01, so that the vents controlling the elevated Fe/Mn in the caldera plumes were not sampled during the *Pisces V* and *ROPOS* dives. What controls the generally elevated Fe/Mn of arc volcanoes relative to MOR hydrothermal systems?

Three processes that could account for elevated Fe and TDFe/TDMn ratios of arc-associated hydrothermal systems have been suggested by Massoth et al. (2003). These processes include: 1) enhanced weathering of host rocks owing to elevated magmatic CO_2 concentrations; 2) enhanced host rock alteration resulting from elevated magmatic H_2S and SO_2; and 3) exsolution of an Fe-rich brine phase. Massoth et al. (2003) suggested that because the hydrothermal plumes at Brothers have TDFe/TDMn values different from whole rock Fe/Mn values the first two processes are likely subordinate in importance to brine exsolution. By contrast, Resing et al. (2007) suggested that enhanced water-rock reaction owing to elevated CO_2, SO_2 and H_2S concentrations (i.e., process 1 and 2 above), most likely controlled the elevated Fe/Mn ratios at NW Rota-1, where the upper plume has TDFe/TDMn values of 14-17, and the lower plume has TDFe/TDMn values up to 120. A compilation of volcanic rock geochemistry from along the Kermadec-Tonga arc shows that felsic rocks along the arc have an average molar Fe/Mn ~ 35, whereas mafic and intermediate rocks have molar Fe/Mn ~ 44 (NIWA & GNS, unpublished data). Butterfield et al. (in press) found that fluids venting at an active volcanic vent at NW Rota-1 had variable Fe/Mn ratios with

maximum values nearly identical to the local basaltic andesite (Fe/Mn near 55), and attribute this to SO_2-driven acid attack on fresh volcanic rock. The Fe/Mn ratio in the NW Rota volcanic vent fluids decreased as the fluid pH increased due to mixing and water/rock reaction.

Although Massoth et al. (2003) favoured phase separation to explain the elevated Fe, the plumes from the Kermadec arc with the most elevated TDFe/TDMn also have the highest ΔpH (i.e., lowest pH) and form a generally positive correlation with host rock molar Fe/Mn (e.g., Fig. 10 of Massoth et al., 2003). Given that large shifts in hydrothermal plume pH require much more acidic vent fluids, these vent fluids would be required to have more elevated $SO_2 \pm H_2S$ concentrations (Resing et al., 2007), which would be the most likely to cause aggressive fluid-rock interaction (Butterfield et al., in press). However, there are several ways in which Fe and Mn might be fractionated from each other: incongruous mineral dissolution; differing pH-redox systematics; the higher probability that Fe (e.g., pyrite, marcasite), not Mn (e.g., alabandite), will precipitate as a sulfide; the differential fluid-mobility of Fe and Mn, and secondary mineral formation (e.g., nontronite). For example, one explanation for the high TDMn relative to TDFe for hydrothermal plume samples at the caldera site is precipitation of Fe-sulfides in the immediate subsurface (Resing et al., 2009); the greater solubility of Mn-sulfides and Mn-chloride complexes (Gammons and Seward, 1996) compared to Fe-sulfides would lower the typically high Fe/Mn of the fluids. The fact that the caldera plume samples range to TDMn values higher than the cone summit plume, yet have lower TDFe, is consistent with diffuse fluids venting at moderate pH from a source that has undergone more water/rock reaction (lower water/rock ratio than the cone summit, which is presumably a highly acidic volcanic vent with properties similar to those seen at NW Rota-1) is consistent with this interpretation and with the presence of pyrite and marcasite in the samples recovered by *ROPOS* in 2007.

Plume sample particulates represent a mixture of hydrothermal, detrital/pelagic, and hydrogenous components. In the context of submarine volcanoes far from the continents, the detrital/pelagic component can be considered as a mixture of pelagic sediment, resuspended volcaniclastic material and primary volcanic ash. Species typically considered hydrothermal include Fe, Mn, Zn, Pb, Cu, whereas detrital species typically include Ti, Al, K, and Na. Iron is added to vent proximal marine sediments by hydrothermal fluids, with a typically strong correlation with P due to adsorption/co-precipitation from seawater (e.g., Feely et al., 1990). Data for ~ 2000 mafic to felsic volcanic rocks from the Kermadec arc and backarc have molar Fe/Al and P/Al of 0.3 ± 0.17 and 0.006 ± 0.005, respectively. These volcanic ratios are essentially the same as average shale; previous studies have shown large enrichment factors in Fe/Al and P/Al with proximity to hydrothermal systems on modern MORs (e.g., Feely et al., 1990). Most of the particulates from Monowai have Fe/Al and P/Al values that exceed these rock values, suggesting that although venting is low-temperature at present, metals have been added to the plumes by hydrothermal fluids. As expected, more robust hydrothermal systems with massive sulfides (e.g., Brothers) have elevated Fe/Al and P/Al compared to Monowai. Elevated Al in the particulates raises the possibility that the CO_2 and SO_2-rich (i.e., highly acidic) nature of some arc hydrothermal systems could result in vent fluids having elevated Al concentrations (i.e., as alunite; de Ronde et al., 2005). Furthermore, although Ti is considered to be immobile in seafloor hydrothermal systems (Baker et al., 2003), the hydrothermal plumes at NW Rota-1 have elevated Ti in the particulates (i.e., elevated Ti/Al and Ti/Fe), suggested to be due to very acidic leaching of the host volcanic rocks (Resing et al., 2007). Essentially all of the particulate samples from Monowai have elevated Ti, up to in excess of the values reported by Resing et al. (2007) (i.e., up to 74.2 nM at the Monowai summit compared to up to 18.3 nM at NW Rota 1). Although the caldera site at Monowai is apparently less acidic and Fe-rich than the cone summit site (Figs. 6, 7), the Ti concentrations

of the particulates from the caldera site (2.0 to 6.6 nM) are well in excess of typical values from MORs and arc systems elsewhere (all < 1 nM, see Table 1 in Baker et al., 2003), with the notable exception of NW Rota-1 (Resing et al., 2007). The elevated Ti for the caldera plume particulates indicates that these plumes are likely related to acidic vent fluids, unlike those sampled at Mussel Ridge. Coincident with the elevated Ti and Al concentrations for the Monowai particulates are elevated Si, S, Na, Mg, Ca, and for the summit cone, K, As, W, Cu, Zn and Pb (Table 2). Therefore, the Monowai cone is essentially a high-sulfidation magmatic-hydrothermal system, in some respects similar to NW Rota-1 and Brothers cone (Resing et al., 2007). The fact that the deeper caldera site has particulates with evidence of more acidic water-rock reactions than suggested by the pH shift is consistent with the anomalously elevated TDMn compared to TDFe, again suggesting significant loss of Fe as sulfide minerals in the subsurface.

Influence of magmatic metals and volatiles

Here we discuss the evidence for a magmatic contribution to the hydrothermal systems at Monowai volcano. de Ronde et al. (2007) suggested that along the southern and mid-Kermadec arc, Macauley and Brothers volcanoes were the only systems where magmatic fluids were clearly implicated in the addition of Fe to the hydrothermal system. Based on the large shifts in pH, elevated TDFe, overall high TDFe/TDMn, and evidence from particles for hydrothermal mobility of Al, Ti, K and Ba, we suggest that Monowai volcano is also an excellent candidate to be considered as a magmatic-hydrothermal system. Further evidence for high volatile contents of the magmatic system includes the formation of a large caldera in an apparently mafic-dominated system; explosive volcanism to produce a caldera at these depths would presumably be more gas-rich, as a function of contributions from dehydration reactions on the subducting Pacific plate.

There is continued discussion regarding the source of metals in seafloor hydrothermal systems and the role of magmatic volatiles in the formation of ore deposits (e.g., de Ronde, 1995; Yang and Scott, 1996; Huston et al., 2001; Beaudoin et al., 2007; Wysoczanski et al., submitted; Timm et al., this volume). Are the metals involved in SMS deposits contributed directly from the degassing magmas in a magma chamber, or are they enriched owing to water-rock interaction during hydrothermal alteration of the surrounding rocks, or do systems evolve with time reflecting contributions from both sources. In other words, is the magma required simply to supply the heat to drive the hydrothermal system, or are metals being supplied directly. By analogy with Brothers volcano, we can speculate that the gas-rich nature of the Monowai fluids, despite relatively low temperatures implies a magmatic contribution. Temperatures at the summit are relatively low at Brothers cone (46 – 122 °C; de Ronde et al., 2011, in press) owing to mixing and dilution by seawater. One of the major differences between arc hydrothermal systems with those associated with MORs is that arc systems are typically more gas-rich because they are typically more felsic and shallower (e.g., de Ronde et al., 2005; de Ronde et al., 2007; Resing et al., 2007). Typically, felsic magmas are also more volatile-rich than mafic magmas because volatiles behave as incompatible elements during magma fractionation, and because felsic magmas are commonly produced by anatexis of more H_2O and CO_2-rich sources than mafic magmas. What is different about the Monowai volcano system is that it appears to be largely a mafic centre. Although there is a lack of information regarding the nature of the crust underneath Monowai volcano, Monowai is located west of the Kermadec Ridge and so is likely largely or entirely constructed on oceanic crust. Although arc mafic rocks are more water-rich than their MOR counterparts, there appears to be little difference in terms of low pH, gas-rich hydrothermal systems on arc volcanoes regardless of the dominant lithology of the host rocks. In other words, despite being mafic, the hydrothermal systems at Monowai appear to

be gas-rich, similar to Brothers and other more felsic systems along the arc (de Ronde et al., 2005; de Ronde et al., 2007) and similar to the dominantly mafic NW Rota-1 system (Resing et al., 2007; Butterfield et al., in press).

On the Kermadec arc closer to New Zealand, thicknesses of sediment cover on the subducting Pacific Plate increases, so that there is evidence from sulfide mineral chemistry at Brothers for a "continental" signature i.e., massive sulfides recovered from the NW caldera site at Brothers are relatively Pb-rich (de Ronde et al., 2005). However, one of the characteristics of arc volcanic rocks is enrichment in Pb over similarly incompatible elements. The extent of Pb enrichment, expressed as $[Pb/Ce]_{MORB}$ averages 9.2 ± 8.5 for the length of the oceanic crustal part of the Kermadec-Tonga arc (NIWA & GNS, unpublished data), with no statistically significant variation with distance from New Zealand. The importance of Pb enrichment in arc systems from the mineral deposit perspective is that volcanic rocks formed from enriched magmas will be relatively Pb-rich, as will the magmas that produced the volcanic rocks. Therefore, regardless of whether magmatic volatiles of rock leaching is the dominant process in supplying metals to hydrothermal fluids, in arc environments, these fluids should be Pb-rich compared to hydrothermal fluids at MORs. Therefore, if massive sulfides are found at Monowai, they are likely to be significantly more Pb-rich than expected from the largely mafic crust and lack of significantly evolved sediment being subducted. Corollary data includes the composition of the particulates.

The alteration and mineralization patterns for rocks and sulfide-sulfate material collected by TV grab, in combination with the occurrence of native sulfur, suggest that the hydrothermal fluids at Monowai caldera were highly acidic and relatively oxidized. The intergrowth of sulfides and sulfates, primarily alunite, reflects cogenetic precipitation and suggests the presence of variable oxidation states of sulfur. The typical platy crystals shape is the characteristic habit of alunite formed in environments with a large magmatic vapour

component in the fluid system (Fig. 10) (Arribas et al., 1995). Probably induced by boiling processes (see below), magmatic SO_2 disproportionates to H_2SO_4 and H_2S or native S, resulting in the coprecipitation of sulfide, native S, and sulfate minerals (Kusakabe et al., 2000; Giggenbach et al., 2003; Butterfield et al., in press). In the near surface, oxidizing environment, H_2SO_4 dissociates further to produce acid, which leads to the formation of characteristic acid-sulfate alteration assemblages. Sulfur isotopes can be used to confirm the disproportionation process, and consequently give evidence for the presence of magmatic volatiles. Due to kinetic effects during disproportionation, the sulfides become enriched in ^{32}S whereas the sulfates are enriched in ^{34}S (Ohmoto and Rye, 1979). Thus, the sulfide/sulfate pairs, precipitated from this fluid, will show different isotope signatures with light sulfur in the sulfide and heavier sulfur in the sulfate species. This effect is documented for Mussel Ridge, where pyrite-alunite pairs of highly altered samples have average $\delta^{34}S$ values of -8.4 ‰ and +7.9 ‰, respectively. The negative isotope signatures require a highly fractionated source of light sulfur, and cannot be explained by leaching from host rocks, which typically have $\delta^{34}S$ values of about 4 ‰ in island arc volcanic rocks. The large difference between the $\delta^{34}S$ of alunite and that of coexisting pyrite, coupled with the highly acid conditions required to stabilize the alunite and pyrophyllite, strongly suggests the involvement of magmatic fluids and gases (Herzig and Hannington, 2000). The isotopic values of native sulfur are close to the magmatic $\delta^{34}S$ signature for island arc volcanic rocks. It seems evident that native sulfur at Mussel Ridge likely formed by direct condensation of magmatic SO_2.

Vent fluids

The vent fluids recovered from the caldera are relatively low temperature (< 60°C) and clearly heavily dominated by seawater (92 to 99% based on Mg). However, the linear trends of dissolved silica and Mn are clear evidence for high-temperature water-rock reaction. The

low-temperature vents (< 60°C) sampled in the caldera include two low-chlorinity sites that are clearly vapour-enriched and five other sites with near-seawater chlorinity. The mixing trends for major elements show a difference between the low-chlorinity fluids and the near-seawater fluids, also consistent with vapour-liquid partitioning (Butterfield et al., 1990) (e.g. Si, Mn, Ca trends are lower for low-Cl fluids than normal-Cl fluids, Fig. 12). This is an indication that phase separation has occurred in the sub-surface, requiring temperatures in excess of 320°C for boiling at the average vent depth of 1100 m. The low vent temperatures and high Mg concentrations indicate a high degree of mixing with seawater-like fluids below the seafloor, with the resultant cooling and neutralization causing precipitation of iron sulphide minerals and resulting in a very low Fe/Mn ratio in the vent fluids. The extrapolation of dissolved silica in vent fluids from 48 mmol/kg to zero mmol/kg magnesium concentration involves considerable uncertainty, but the resulting 16.9 mmol/kg end member silica would require reaction zone conditions of 350°C and 300 bars (Von Damm 1991). The vent fluids have high total dissolved sulphur, strongly suggesting addition of magmatic sulphur gas.

The prevalence of extruded sulphur, alunite and pyrite at the low-temperature vents requires a period of strongly acidic, high-temperature venting at this site. The $\delta^{34}S$ values for the pyrite-alunite minerals suggests venting temperatures were at least ~ 300°C. Furthermore, altered and mineralized basaltic andesites from Mussel Ridge show progressive enrichment in high-temperature fluid-associated metals (with the notable exception of Zn), including Pb, Mo, As, Au, Cu, Sb and Sn (Fig. 11; Table 3), consistent with apparently high temperature pyrite + alunite along with pyrophyllite (Fig. 10), implying elevated fluid temperatures (280-300°C; Reyes, 1990). Thus, the alteration assemblage (pyrite + alunite ± pyrophyllite), gas-rich nature of the vent fluids, low Fe/Mn values of the vent fluids and plumes, and low salinity of the end member hydrothermal fluid owing to phase separation suggests that there

is a high temperature reaction zone in the subsurface proximal to the southern wall of the caldera, and that much of the metal budget may have been lost in the subsurface via sulfide mineral deposition.

For the Monowai cone summit, no vent fluids have been collected. However, the composition of the plume is consistent with venting of a strongly acidic, gas- and metal-rich fluid comparable to volcanic vent fluids observed at NW Rota-1 (Butterfield et al., in press). The elevated CH_4/Mn, Fe/Mn and TDMn and TDFe are consistent with magmatic inputs associated with recent and on-going volcanic activity, as also observed at NW Rota-1 and West Mata. Although both the Monowai cone and caldera hydrothermal systems are volatile-rich, there are clear and significant differences in the compositions of the associated hydrothermal plumes. These differences suggest either different pathways (i.e., length and tortuosity) for magmatic and hydrothermal fluids from depth to the seafloor, as recently suggested for Brothers volcano (de Ronde et al., 2011, in press) or two separate magma chambers, as suggested by Timm et al (Timm et al., 2011 in press) for the MVC and consistent with the more mafic character of Monowai cone compared to volcanic rocks at Mussel Ridge.

Conclusions

The Kermadec arc is probably the most hydrothermally active submarine volcanic system in the world. The Monowai Volcanic Centre, located at the mid-point along the ~2530 km long Tonga-Kermadec arc system, is comprised of a large elongate caldera (7.9 x 5.7 km; 35 km^2; floor depth of the caldera is 1590 m), which has formed within an older caldera some 84 km^2 in area. To the south of the new caldera there is a large stratovolcano, which rises to within < 150 m of the seafloor and has been volcanically active for at least several decades. Unlike most of the calderas along the arc, mafic volcanic rocks dominate the MVC. Plume

mapping during the 2004 NZAPLUME III cruise has revealed at least 3 major hydrothermal systems associated with the caldera and cone, in addition to a number of smaller plumes. Monowai cone has venting from the summit, as well as several plumes down the northern flank of the volcano. The lack of ^{3}He anomalies associated with these smaller flank plumes indicates that these are not hydrothermal in origin. The caldera has a major hydrothermal vent system associated with the southwest wall of the caldera. The summit plume is gas-rich and acidic; plume samples show a pH shift of -2.00 ph units, H_2S up to 32 μM and CH_4 concentrations up to 900 nM. The summit plume has elevated total dissolvable Fe (TDFe up to 4200 nM), TDMn (up to 412 nM), and TDFe/TDMn (up to 20.4). In contrast, the caldera plumes have lower TDFe, but range to higher TDMn concentrations, and are relatively gas-poor (no H_2S detected, pH shift of -0.06 pH units, CH_4 concentrations up to 26 nM). Elevated TDMn and generally lower TDFe/TDMn values for the caldera plumes compared to those on the cone are interpreted to be the result of significant precipitation of Fe-sulfides in the subsurface, raising the distinct possibility for the occurrence of shallow buried massive sulfide mineralization at Monowai.

This interpretation is generally consistent with the observed vent fluid chemistry from the caldera. The vent fluids high total dissolved sulphur (sulphate plus sulphide) consistent with the addition of a magmatic sulphur gas at depth within the caldera. The elevated Mn content of the vent fluids indicates significant water/rock reaction has taken place, and the low iron content is consistent with precipitation of iron sulphides below the seafloor. However, the fluids have Fe/Mn ratios much lower than observed in the caldera plume, and the plumes extend 150 m deeper than the deepest observed vents, so there must be additional unsampled vent fluid sources to the caldera plumes.

Particulate samples from both the cone sites and the caldera site are enriched in Al, Ti, Ca, Mg, Si, and S, with the cone summit plume particularly enriched in K, As, W and Cu, Pb,

Zn. The elevated Ti and Al suggest acidic water-rock reactions and intense high-sulfidation like alteration of the host volcanic rocks. Observations from submersible dives with *Pisces V* in 2005 of the caldera site indicate numerous low temperature vents (< 60°C), with a large biomass of vent-associated fauna, in particular large accumulations of the mussel *Bathymodiolus* sp. and the tubeworm *Lamellibrachia* sp.

We interpret the Monowai cone as possessing a robust high-sulfidation magmatic-hydrothermal system. The large shifts in pH, elevated TDFe and TDFe/TDMn, H_2S-rich nature of the vent fluids and elevated Ti and Al in the particulates indicates significant magmatic volatile ± metal contributions to the hydrothermal system. The differences and similarities between the plumes at the summit of Monowai cone and the caldera site suggest active Fe-sulfide formation in the subsurface, and the potential for the presence of significant SMS mineralization at depth, consistent with vent fluids at the caldera having undergone phase separation and with the presence of high temperature alteration mineral assemblage (pyrite + alunite ± pyrophyllite).

Acknowledgments

The NZAPLUME III cruise on the R/V *Tangaroa* was jointly funded by NZ Government grants to GNS Science and NIWA. Funding for the New Zealand American Submarine Ring of Fire 05 expedition was provided from the NOAA VENTS Program, the NOAA Office of Ocean Exploration and Research (OER), GNS Science, and NIWA. NOAA's Undersea Research Program (NURP) provided funding for some of the transit time from Hawaii to New Zealand that made the entire expedition possible (there were several other legs of the expedition). The Hawaii Undersea Research Laboratory very capably operated the *Pisces V* submersible and the RCV-150 remotely operated vehicle used on this expedition. The R/V *Ka'imikai-o-Kanaloa* provided excellent support for the operation. Funding for the SO192-2

MANGO cruise on the R/V *Sonne* was provided by the German Federal Ministry of Education and Research (grant# 03G0192). Thanks are also due to the crew onboard FS *Sonne* and the excellent performance of the *ROPOS* crew. We thank journal reviewers xxxx and yyyy for their constructive comments that greatly improved the paper. Pacific Marine Environmental Laboratory contribution #3175.

REFERENCES

Arribas, A., Cunningham, C. G., Rytuba, J. J., Rye, R. O., Kelly, W. C., Podwysocki, M. H., Mckee, E. H., and Tosdal, R. M., 1995, Geology, Geochronology, Fluid Inclusions, and Isotope Geochemistry of the Rodalquilar Gold Alunite Deposit, Spain: Economic Geology and the Bulletin of the Society of Economic Geologists, v. 90, p. 795-822.

Baker, E. T., Embley, R. W., Walker, S. L., Resing, J. A., Lupton, J. E., Nakamura, K. I., de Ronde, C. E. J., and Massoth, G. J., 2008, Hydrothermal activity and volcano distribution along the Mariana arc: Journal of Geophysical Research B: Solid Earth, v. 113.

Baker, E. T., Feely, R. A., De Ronde, C. E. J., Massoth, G. J., and Wright, I. C., 2003, Submarine hydrothermal venting on the southern Kermadec volcanic arc front (offshore New Zealand): Location and extent of particle plume signatures, Geological Society Special Publication, p. 141-161.

Beaudoin, Y., and Scott, S. D., 2009, Pb in the PACMANUS sea-floor hydrothermal system, eastern Manus Basin; numerical modeling of a magmatic versus leached origin: Economic Geology, v. 104, p. 749-758.

Beaudoin, Y., Scott, S. D., Gorton, M. P., Zajacz, Z., and Halter, W., 2007, Effects of hydrothermal alteration on Pb in the active PACMANUS hydrothermal field, ODP Leg 193, Manus Basin, Papua New Guinea; a LA-ICP-MS study: Geochimica et Cosmochimica Acta, v. 71, p. 4256-4278.

Bennett, S. A., Achterberg, E. P., Connelly, D. P., Statharn, P. J., Fones, G. R., and German, C. R., 2008, The distribution and stabilisation of dissolved Fe in deep-sea hydrothermal plumes: Earth and Planetary Science Letters, v. 270, p. 157-167.

Butterfield, D. A., Massoth, G. J., McDuff, R. E., Lupton, J. E., and Lilley, M. D., 1990, Geochemistry of hydrothermal fluids from Axial Seamount hydrothermal emissions study vent field, Juan de Fuca Ridge: subseafloor boiling and subsequent fluid-rock interaction: Jour. Geophys. Res., v. 95, p. 12895-12921.

Butterfield, D. A., Nakamura, K.-I., Takano, B., Lilley, M. D., Lupton, J. E., Resing, J. A., and Roe, K. K., in press, High SO_2 flux, sulfur accumulation, and gas fractionation at an erupting submarine volcano: Geology.

Chadwick, W. W., Jr., Wright, I. C., Schwarz-Schampera, U., Hyvernaud, O., Reymond, D., and de Ronde, C. E. J., 2008, Cyclic eruptions and sector collapses at Monowai submarine volcano, Kermadec arc: 1998,Äì2007: Geochem. Geophys. Geosyst., v. 9.

Cowen, J. P., Massoth, G. J., and Feely, R. A., 1990, Scavenging rates of dissolved manganese in a hydrothermal vent plume: Deep-Sea Research, v. Part A: Oceanographic Research Papers. 37, p. 1619-1637.

Davey, F. J., 1980, The Monowai seamount: an active submarine volcanic centre on the Tonga—Kermadec ridge: New Zealand Journal of Geology and Geophysics, v. 23, p. 533-536.

de Ronde, C., Baker, E., Embley, R., Lupton, J., Butterfield, D., Faure, K., Leybourne, M., Chadwick, W., Ishibashi, J., Resing, J., Walker, S., Merle, S., and Greene, R., 2009, Hydrothermal systems of intraoceanic arcs: Geochimica Et Cosmochimica Acta, v. 73, p. A282-A282.

de Ronde, C. E. J., 1995, Fluid chemistry and isotopic characteristics of seafloor hydrothermal system and associated VMS deposits; potential for magmatic contributions: Short Course Handbook, v. 23, p. 479-509.

de Ronde, C. E. J., Baker, E. T., Massoth, G. J., Lupton, J. E., Wright, I. C., Feely, R. A., and Greene, R. R., 2001, Intra-oceanic subduction-related hydrothermal venting,

Kermadec volcanic arc, New Zealand: Earth and Planetary Science Letters, v. 193, p. 359-369.

de Ronde, C. E. J., Baker, E. T., Massoth, G. J., Lupton, J. E., Wright, I. C., Sparks, R. J., Bannister, S. C., Reyners, M. E., Walker, S. L., Greene, R. R., Ishibashi, J., Faure, K., Resing, J. A., and Lebon, G. T., 2007, Submarine hydrothermal activity along the mid-Kermadec Arc, New Zealand: large-scale effects on venting: Geochemistry, Geophysics, Geosystems, v. 8, p. Q07007.

de Ronde, C. E. J., Hannington, M. D., Stoffers, P., Wright, I. C., Ditchburn, R. G., Reyes, A. G., Baker, E. T., Massoth, G. J., Lupton, J. E., Walker, S. L., Greene, R. R., Soong, C. W. R., Ishibashi, J., Lebon, G. T., Bray, C. J., and Resing, J. A., 2005, Evolution of a submarine magmatic-hydrothermal system: Brothers volcano, southern Kermadec arc, New Zealand: Economic Geology, v. 100, p. 1097-1133.

de Ronde, C. E. J., Massoth, G. J., Butterfield, D. A., Christenson, B. W., Ishibashi, J., Ditchburn, R. G., Hannington, M. D., Brathwaite, R. L., Lupton, J. E., Kamenetsky, V. S., Graham, I. J., Zellmer, G. F., Dziak, R. P., Embley, R. W., Dekov, V. M., Munnik, F., Lahr, J., Evans, L. J., and Takai, K., 2011, in press, Submarine hydrothermal activity and gold-rich mineralization at Brothers Volcano, Kermadec arc, New Zealand: Mineralium Deposita.

DeMets, C., Gordon, R. G., Argus, D. F., and Stein, S., 1994, Effect of recent revisions to the geomagnetic reversal time scale and estimates of current plate motions: Geophysical Research Letters, v. 21, p. 2191-2194.

Edmond, J. M., Measures, C., McDuff, R. E., Chan, L. H., Collier, R., and Grant, B., 1979, Ridge crest hydrothermal activity and the balances of the major and minor elements in the ocean: the Galapagos data: Earth Planet. Sci. Lett., v. 46, p. 1-19.

Embley, R. W., de Ronde, C. E. J., Massoth, G. J., and Participants, S., 2006, New Zealand American Submarine Ring of Fire 2005—Kermadec arc submarine volcanoes: Cruise Report.

Feely, R. A., Massoth, G. J., Baker, E. T., Cowen, J. P., Lamb, M. F., and Krogslund, K. A., 1990, The Effect of Hydrothermal Processes on Midwater Phosphorus Distributions in the Northeast Pacific: Earth and Planetary Science Letters, v. 96, p. 305-318.

Gammons, C. H., and Seward, T. M., 1996, Stability of manganese(II) chloride complexes from 25 to 300 degrees C: Geochimica et Cosmochimica Acta, v. 60, p. 4295-4311.

Gharib, J. J., Sansone, F. J., Resing, J. A., Baker, E. T., Lupton, J. E., and Massoth, G. J., 2005, Methane dynamics in hydrothermal plumes over a superfast spreading center: East Pacific Rise, 27.5 degrees-32.3 degrees S: Journal of Geophysical Research-Solid Earth, v. 110, p. -.

Giggenbach, W. F., Shinohara, H., Kusakabe, M., and Ohba, T., 2003, Formation of acid volcanic brines through interaction of magmatic gases, seawater, and rock within the White Island volcanic-hydrothermal system, New Zealand: Special Publication (Society of Economic Geologists (U S)), v. 10, p. 19-40.

Graham, I. J., Reyes, A. G., Wright, I. C., Peckett, K. M., Smith, I. E. M., and Arculus, R. J., 2008, Structure and petrology of newly discovered volcanic centers in the northern Kermadec-southern Tofua arc, South Pacific Ocean: Journal of Geophysical Research B: Solid Earth, v. 113.

Haase, K. A., Stroncik, N., Garbe-Schnoberg, D., and Stoffers, P., 2006, Formation of island arc dacite magmas by extreme crystal fractionation: An example from Brothers Seamount, Kermadec island arc (SW Pacific): Journal of Volcanology and Geothermal Research, v. 152, p. 316-330.

Haase, K. M., Worthington, T. J., Stoffers, P., Garbe-Sch√∂nberg, D., and Wright, I., 2002, Mantle dynamics, element recycling, and magma genesis beneath the Kermadec Arc-Havre Trough: Geochem. Geophys. Geosyst., v. 3.

Hannington, M. D., Jonasson, I. R., Herzig, P. M., and Petersen, S., 1995, Physical and chemical processes of seafloor mineralization at mid-ocean ridges: Geophysical Monograph, v. 91, p. 115-157.

Herzig, P. M., and Hannington, M. D., 2000, Chapter 13. Input from the deep: Hot vents and cold seeps, *in* Schulz, H. D., and Zabel, M., eds., Marine Geochemistry: Berlin, Springer-Verlag, p. 398-416.

Huston, D. L., Brauhart, C. W., Drieberg, S. L., Davidson, G. J., and Groves, D. I., 2001, Metal leaching and inorganic sulfate reduction in volcanic-hosted massive sulfide mineral systems: Evidence from the paleo-Archean Panorama district, Western Australia: Geology, v. 29, p. 687-690.

Kadko, D. C., Rosenberg, N. D., Lupton, J. E., Collier, R. W., and Lilley, M. D., 1990, Chemical-Reaction Rates and Entrainment within the Endeavor Ridge Hydrothermal Plume: Earth and Planetary Science Letters, v. 99, p. 315-335.

Kusakabe, M., Komoda, Y., Takano, B., and Abiko, T., 2000, Sulfur isotopic effects in the disproportionation reaction of sulfur dioxide in hydrothermal fluids: implications for the delta S-34 variations of dissolved bisulfate and elemental sulfur from active crater lakes: Journal of Volcanology and Geothermal Research, v. 97, p. 287-307.

Lupton, J. E., Lilley, M., Butterfield, D., Evans, L., Embley, R. W., Massoth, G., Christenson, B., Nakamura, K. I., and Schmidt, M., 2008, Venting of a separate CO2-rich gas phase from submarine arc volcanoes: Examples from the Mariana and Tonga-Kermadec arcs: Journal of Geophysical Research B: Solid Earth, v. 113.

Massoth, G. J., de Ronde, C. E. J., Lupton, J. E., Feely, R. A., Baker, E. T., Lebon, G. T., and Maenner, S. M., 2003, Chemically rich and diverse submarine hydrothermal plumes of the southern Kermadec volcanic arc (New Zealand): Geological Society Special Publications, v. 219, p. 119-139.

Ohmoto, H., and Lasaga, A., 1982, Kinetics of reactions between aqueous sulfates and sulfides in hydrothermal systems: Geochimica et Cosmochimica Acta, v. 46, p. 1727-1745.

Ohmoto, H., and Rye, R. O., 1979, Isotopes of Sulfur and Carbon, *in* Barnes, H. L., ed., Geochemistry of Hydrothermal Ore Depostis: New York, Wiley, p. 509-567.

Resing, J. A., Baker, E. T., Lupton, J. E., Walker, S. L., Butterfield, D. A., Massoth, G. J., and Nakamura, K.-i., 2009, Chemistry of hydrothermal plumes above submarine volcanoes of the Mariana Arc: Geochemistry Geophysics Geosystems, v. 10.

Resing, J. A., Lebon, G., Baker, E. T., Lupton, J. E., Embley, R. W., Massoth, G. J., Chadwick, W. W., Jr., and de Ronde, C. E. J., 2007, Venting of acid-sulfate fluids in a high-sulfidation setting at NW Rota-1 submarine volcano on the Mariana Arc: Economic Geology and the Bulletin of the Society of Economic Geologists, v. 102, p. 1047-1061.

Reyes, A. G., 1990, Petrology of Philippine geothermal systems and the application of alteration mineralogy to their assessment: Journal of Volcanology and Geothermal Research, v. 43, p. 279-309.

Schwarz-Schampera, U., Botz, R., Hannington, M., Adamson, R., Anger, V., Cormany, D., Evans, L., Gibson, H., Haase, K., Hirdes, W., Hocking, M., Juniper, K., Langley, S., Leybourne, M., Metaxis, A., Mills, R., Ostertag-Henning, C., Rauch, M., Rutkowski, J., Schmidt, M., Sheperd, K., Stevens, C., Tamburri, K., Tracey, D., and Weternstroer, U., 2007, Cruise report Sonne 192/2 MANGO, 11280/07: Hannover, BGR, Bundesanstalt für Geowissenschaften und Rohstoffe, p. 92.

Schwarz-Schampera, U., Botz, R., Hannington, M., Evans, L., Gibson, H., Haase, K., Hirdes, W., Hocking, M., Juniper, K., Langley, S., Leybourne, M., Metaxis, A., Ostertag-Henning, C., Rauch, M., Rutkowski, J., Schmidt, M., Sheperd, K., Stevens, C., and Tracey, D., 2008, Status Report 2008 Sonne 192/2 - MANGO, 10924/08: Hannover, BGR, Bundesanstalt für Geowissenschaften und Rohstoffe, p. 41.

Seyfried, J., W.E., 1987, Experimental and theoretical constraints on hydrothermal alteration processes at mid-ocean ridges: Annual Review of Earth and Planetary Sciences, v. 15, p. 317-336.

Stanton, R. L., 1991, Understanding volcanic massive sulfides - Past, Present, and Future, *in* Hutchinson, R. W., and Grauch, R. I., eds., Historical Perspectives of Genetic Concepts and Case Histories of Famous Discoveries(8): New Haven, CT, Economic Geology Publishing Company, p. 82-95.

Statham, P. J., German, C. R., and Connelly, D. P., 2005, Iron(II) distribution and oxidation kinetics in hydrothermal plumes at the Kairei and Edmond vent sites, Indian Ocean: Earth and Planetary Science Letters, v. 236, p. 588-596.

Stoffers, P., Wright, I. C., and Party, a. t. S. S., 1999, Cruise report Sonne 135, Havre Trough-Taupo Volcanic Zone: Tectonic , magmatic and hydrothermal processes, Suva-Fiji-Wellingtn, New Zealand, Sept. 9 - Oct. 15, 1998: Berichte-Reports, Institut für Geowissenschaften, Universität Kiel, v. Nr. 1, p. 77.

Timm, C., de Ronde, C. E. J., Leybourne, M. I., Layton-Mathews, D., and Graham, I., this volume, Source of chalcophile and siderophile elements in Kermadec arc rocks and its contribution to seafloor oceanic arc hydrothermal SMS deposits: Economic Geology.

Timm, C., Graham, I. J., de Ronde, C. E. J., Leybourne, M. I., and Woodhead, J., 2011 in press, Geochemical evolution of Monowai: new insights into the northern Kermadec arc subduction system, SW Pacific: Geochemistry, Geophysics, Geosystems.

Verma, M. P., 2008, Qrtzgeotherm: An ActiveX component for the quartz solubility geothermometer: Computers & Geosciences, v. 34, p. 1918-1925.

Walker, S. L., Baker, E. T., Leybourne, M. I., de Ronde, C. E. J., Greene, R., Faure, K., Chadwick, W., Dziak, R. P., Lupton, J., and Lebon, G., 2010, Transport of Fine Ash Through the Water Column at Erupting Volcanoes – Monowai Cone, Kermadec-Tonga Arc, Kermadec Arc: AGU Fall Meeting, p. Abstract #T13B-2193.

Walker, S. L., Baker, E. T., Resing, J. A., Chadwick, W. W., Lebon, G. T., Lupton, J. E., and Merle, S. G., 2008, Eruption-fed particle plumes and volcaniclastic deposits at a submarine volcano: NW Rota-1, Mariana Arc: Journal of Geophysical Research-Solid Earth, v. 113, p. -.

Wright, I. C., Chadwick Jr, W. W., de Ronde, C. E. J., Reymond, D., Hyvernaud, O., Gennerich, H. H., Stoffers, P., Mackay, K., Dunkin, M. A., and Bannister, S. C., 2008, Collapse and reconstruction of Monowai submarine volcano, Kermadec arc, 1998-2004: Journal of Geophysical Research B: Solid Earth, v. 113.

Wright, I. C., Parson, L. M., and Gamble, J. A., 1996, Evolution and interaction of migrating cross-arc volcanism and backarc rifting: An example from the southern Havre Trough (35 degrees 20'-37 degrees S): Journal of Geophysical Research-Solid Earth, v. 101, p. 22071-22086.

Wysoczanski, R. J., Handler, M. R., Schipper, C. I., Leybourne, M. I., Creech, J., Rotella, M. D., Nichols, A. R. L., Wilson, C. J. N., and Stewart, R. B. S. I. o. E. G., submitted, The magmatic source of SMS- related metal and volatile elements in the southern Kermadec Arc: Economic Geology.

Yang, K., and Scott, S. D., 2002, Magmatic degassing of volatiles and ore metals into a hydrothermal system on the modern sea floor of the eastern Manus back-arc basin, western Pacific: Economic Geology, v. 97, p. 1079-1100.

Yang, K. H., and Scott, S. D., 1996, Possible contribution of a metal-rich magmatic fluid to a sea-floor hydrothermal system: Nature, v. 383, p. 420-423.

FIGURE CAPTIONS

Figure 1. Location and tectonic setting of the Monowai volcanic center at the northern end of the Kermadec arc. A) Regional tectonic setting of the Kermadec–Tonga arc system with the associated Havre trough and Lau basin backarc systems. The older remnant arcs are represented by the Colville–Lau ridges. Relative motions for the Pacific–Australian plates in mm/yr shown by arrows (DeMets et al., 1994). The Kermadec and Tonga arc-front sectors are (south to north): Taupo Volcanic Zone (TVZ); southern Kermadec arc (SKA); middle Kermadec arc (MKA; S = southern part; N = northern part); northern Kermadec arc (NKA); southern Tonga arc (STA). B) Expanded view of the Kermadec arc, showing hydrothermally active submarine volcanic centres.

Figure 2. Detailed bathymetric map of Monowai volcanic center. Also show are locations of dredge tracks, tow-yos and vertical casts. Bathymetry collected by Simrad EM300, R/V *Tangaroa*, 2004.

Figure 3. Geology of the southwest caldera hydrothermal vent site at Monowai volcano, constructed from observations from four *Pisces V* dives of the area. Active venting is mainly focussed on Mussel Ridge. Some chimney structures were observed, including sulfur chimneys, but most vents were not associated with chimneys. EM300 data were provided courtesy of NIWA.

Figure 4. Photos of Monowai caldera hydrothermal systems taken during *Pisces V* dives, 2005. A) Barnacle-encrusted pillow tubes. B) Cross section of pillow tube with relatively light dusting of sediment. C) Low-temperature vent with native sulfur. D) Low temperature vent with native sulfur and tube worms. E) Tube-worms, mussels and crabs from Mussel Ridge. F) Mound covered with mussels, crabs and anemones.

Figure 5. Particle plume distributions at Monowai volcanic center during the NZAPLUME III survey in 2004. The saw-toothed tow-path of the CTDO during tow-yos is shown (light

gray lines). Locations of the tow-yos are shown in figure 2. The ΔNTU scale applies to all panels. Note that a large portion of the caldera plume (roughly 1050-1400m) is below the depth of the observed vents (roughly 1170 to 1050m) indicating that there is a deeper source of venting than sampled by *Pisces* or *ROPOS*. Restricted circulation below the sill depth will likely prevent dissipation of the caldera plume.

Figure 6. Plots of pH versus depth for the vertical casts and tow-yos over the Monowai volcanic centre. Samples are colour-coded with proportional symbol sizes based on the LSS measurements during continuous CTDO operations. A) All data, and B) zoom to exclude the low pH Monowai volcano cone samples. Key features are that shallow samples from the cone have large shifts in pH (-2.00 pH units), samples from the caldera (> 1000 m) also have significant, although smaller, pH shifts (around -0.06 pH units). [The particle plume at 600 m depth has no apparent pH shift and no Mn as noted in the text].

Figure 7. Plots of hydrothermal plume samples from tow-yos and casts across Monowai caldera and cone, showing the relationships between pH and total dissolvable metals. There is a strong dependence of TDFe on pH in the shallow plume over the summit cone, but little to no correlation within the flank plumes or the caldera plume. Note the strong correlation between particulate and total dissolvable Fe. Also note that plume samples from Monowai cone have the most elevated total dissolvable metals concentrations, coincident with anomalously elevated CH_4 (Fig. 9).

Figure 8. Depth plots for A) TDFe, B) TDMn, C) LSS, and D) TDFe/TDMn. Note that the three major plume sources (cone summit, 600 m depth on cone flank, and caldera) have different chemical characteristics. See text for details.

Figure 9. Plots of hydrothermal plume samples from tow-yos and casts across Monowai caldera and cone, showing the relationships between A, B) total dissolvable metals and methane, and C) depth and δ^3He. Several plume samples from Monowai cone summit

plume have anomalously elevated CH_4 concentrations, although many samples from the cone and caldera sites are also elevated over regional (non-hydrothermal) background.

Figure 10. Mineralogical characterization of samples from the Monowai volcano by SEM. A: Natrojarosite crystals as open space fillings [26TVG02I]. B: Natroalunite in SiO_2-rich matrix [26TVG01I]. C, D: Close intergrowths of pyrite with natroalunite [26TVG02 and 26TVG01IV]. E, F: Intergrowths of marcasite and pyrite in a matrix of amorphous silica and alunite [26TVG01].

Figure 11. N-type MORB-normalized plot for average volcanic glass (n = 7), least-altered (n = 15), and mineralized (n = 21) basalts and basaltic andesites, and alteration crusts (n = 5) (n = 3) and native sulphur precipitates from the Mussel Ridge, Monowai caldera. Note the enrichment in Pb, Sb, and Mo for the mineralized samples.

Figure 12. Plots of selected vent fluid chemical variables versus Mg for Monowai caldera. Although dominated by the seawater end member, the effects of both mixing with seawater and phase separation are evident.

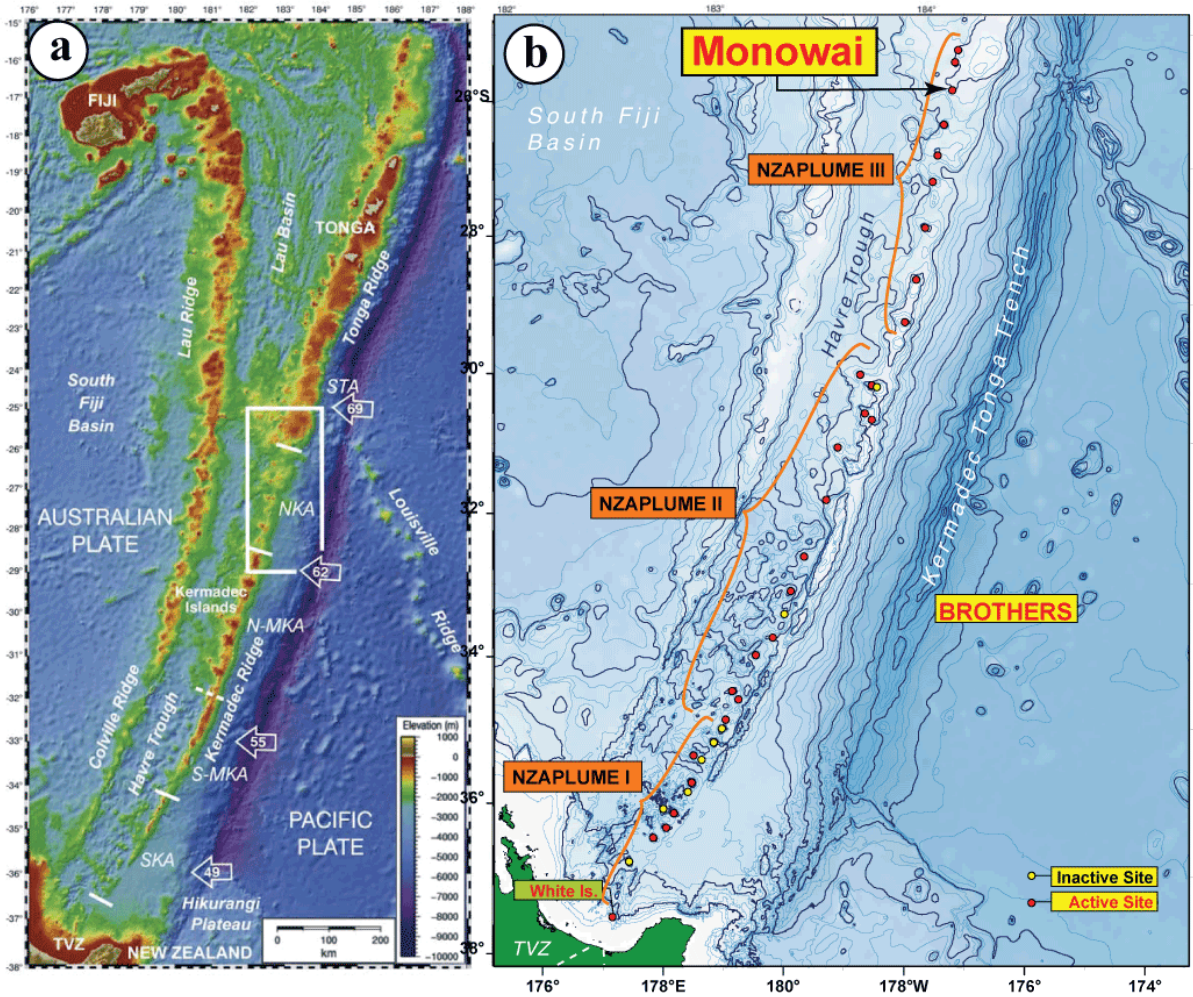

Figure 1. Leybourne et al

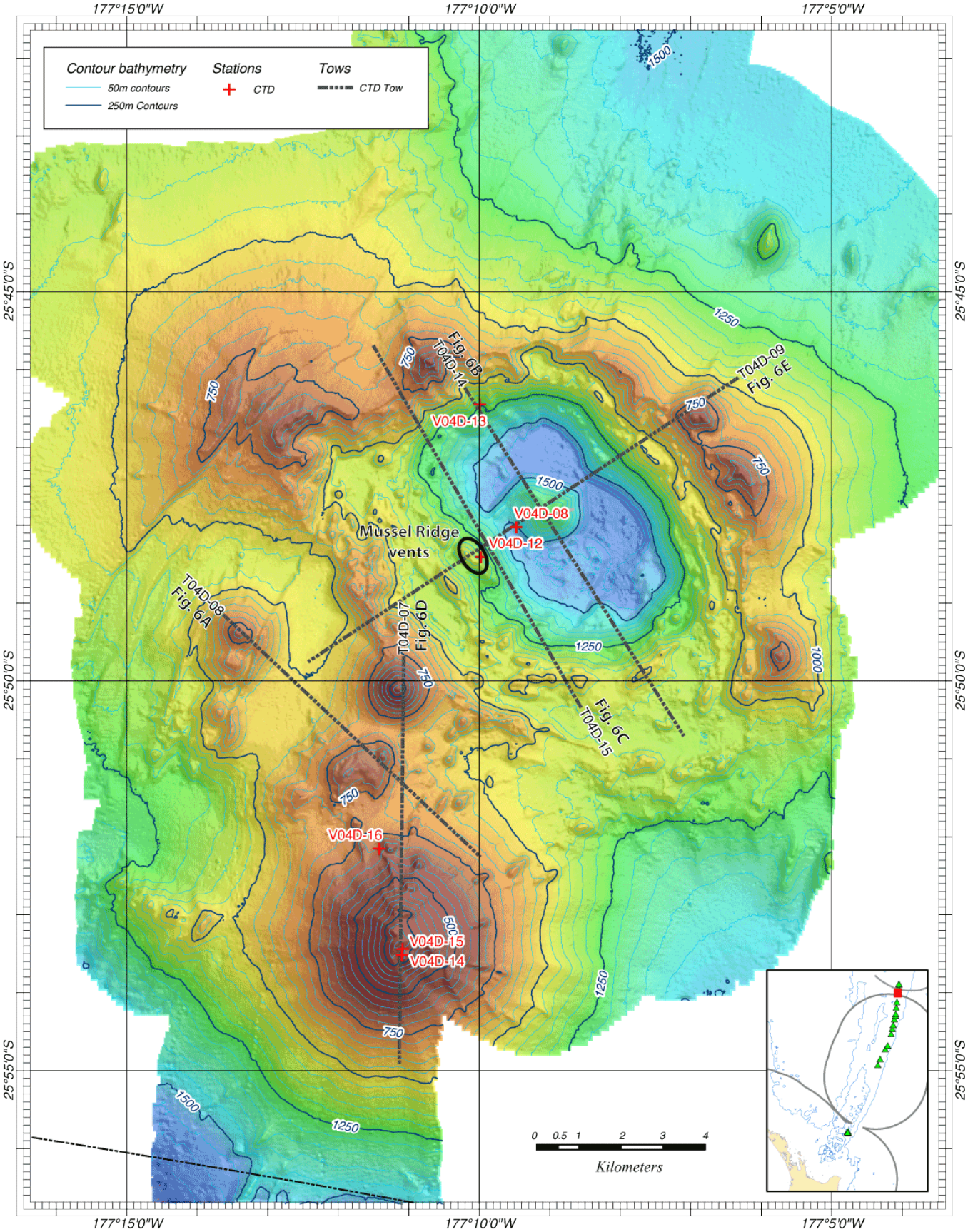

Figure 2. Leybourne et al

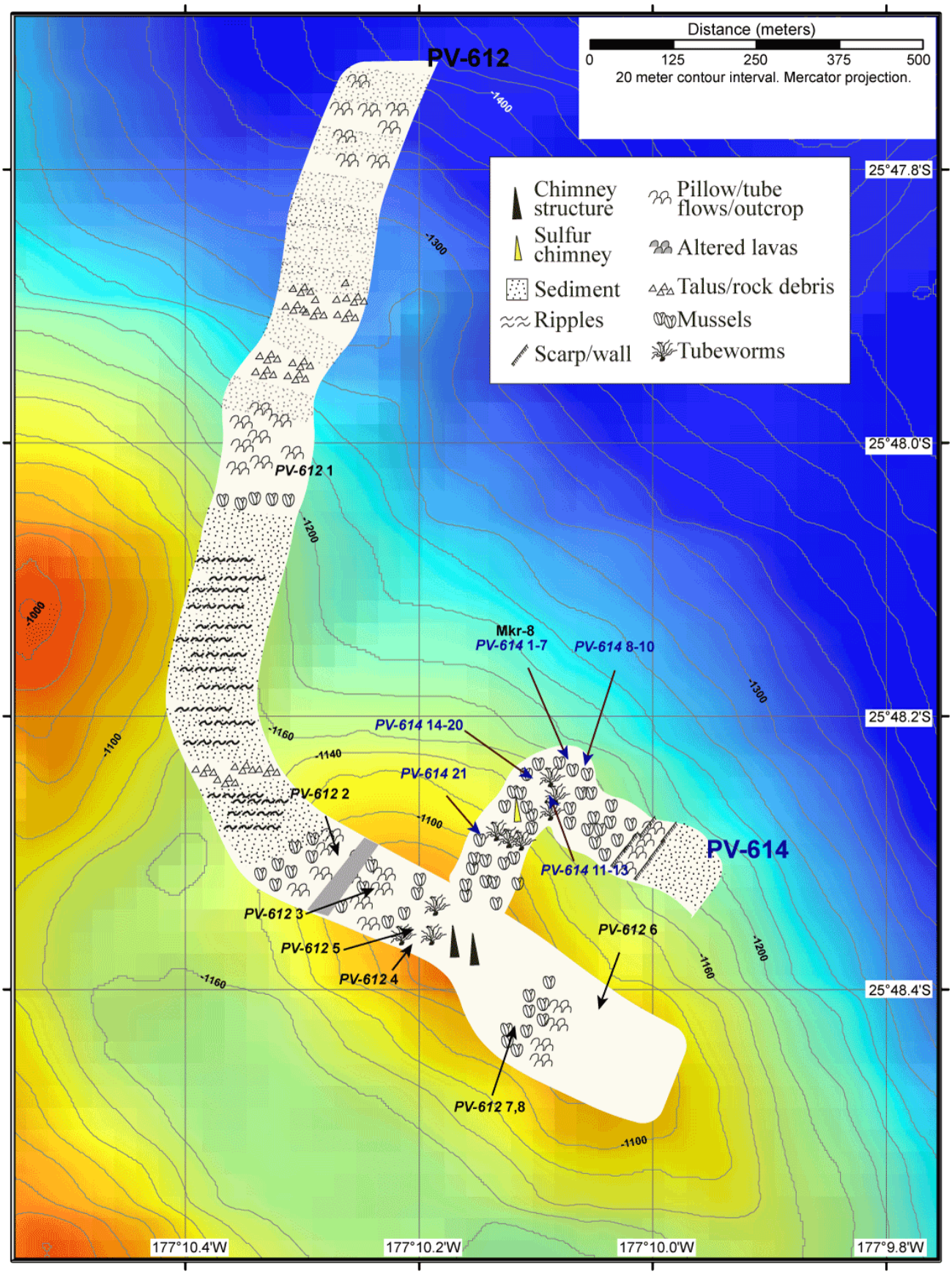
Distance (meters)
0
125
250
375
500
20 meter contour interval. Mercator projection.
Chimney structure
Sulfur chimney
Sediment
Ripples
Scarp/wall
Pillow/tube flows/outcrop
Altered lavas
Talus/rock debris
Mussels
Tubeworms
PV-612
PV-614
PV-612 1
PV-612 2
PV-612 3
PV-612 4
PV-612 5
PV-612 6
PV-612 7,8
Mkr-8
PV-614 1-7
PV-614 8-10
PV-614 11-13
PV-614 14-20
PV-614 21
-1400
-1300
-1200
-1160
-1140
-1100
-1000
25°47.8'S
25°48.0'S
25°48.2'S
25°48.4'S
177°10.4'W
177°10.2'W
177°10.0'W
177°9.8'W

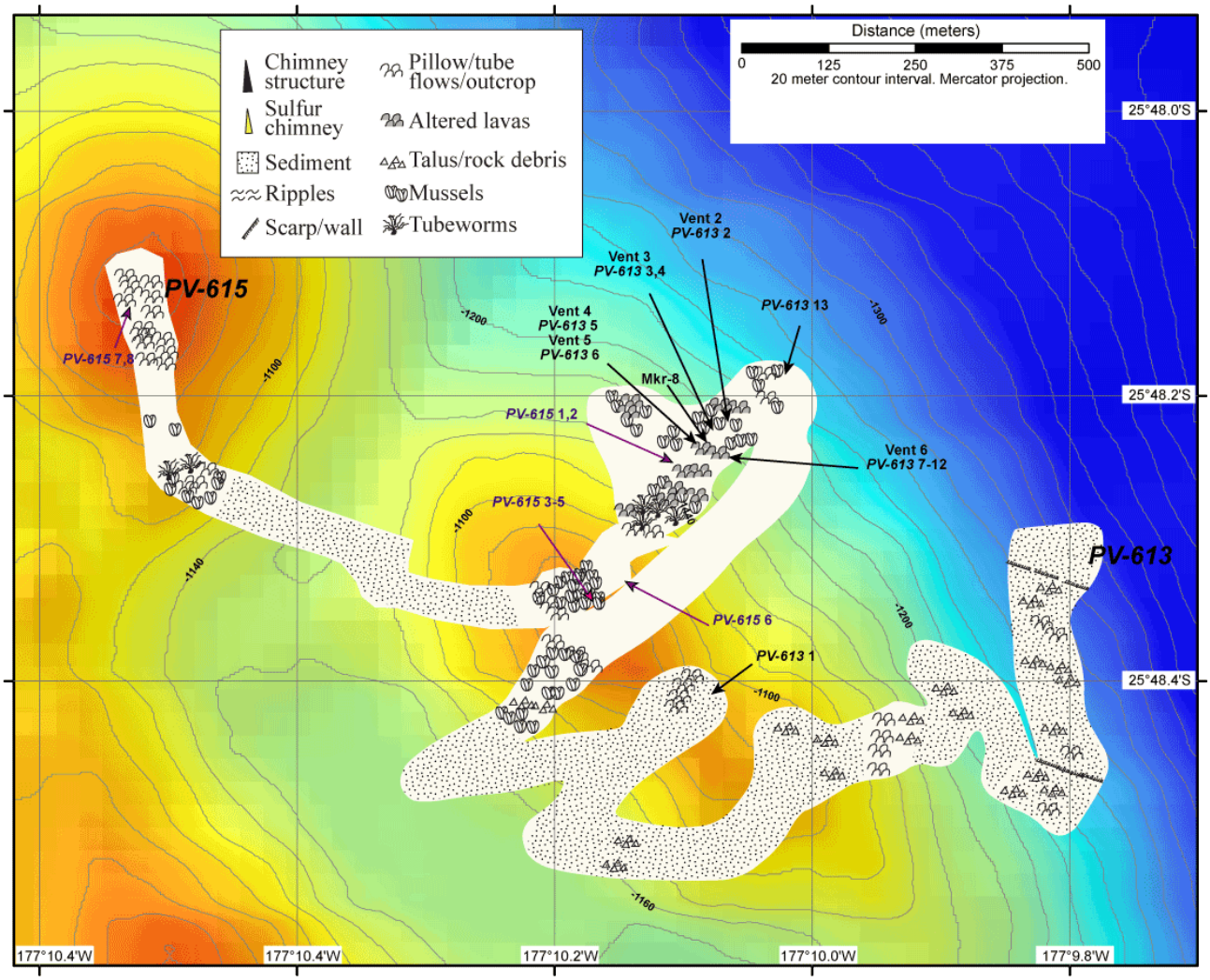
Chimney structure
Sulfur chimney
Sediment
Ripples
Scarp/wall
Pillow/tube flows/outcrop
Altered lavas
Talus/rock debris
Mussels
Tubeworms
Distance (meters)
0
125
250
375
500
20 meter contour interval. Mercator projection.
PV-615
PV-613
PV-615 7,8
PV-615 1,2
PV-615 3-5
PV-615 6
PV-613 1
PV-613 13
Vent 2
PV-613 2
Vent 3
PV-613 3,4
Vent 4
PV-613 5
Vent 5
PV-613 6
Mkr-8
Vent 6
PV-613 7-12
-1100
-1140
-1200
-1300
-1160
25°48.0'S
25°48.2'S
25°48.4'S
177°10.4'W
177°10.4'W
177°10.2'W
177°10.0'W
177°9.8'W

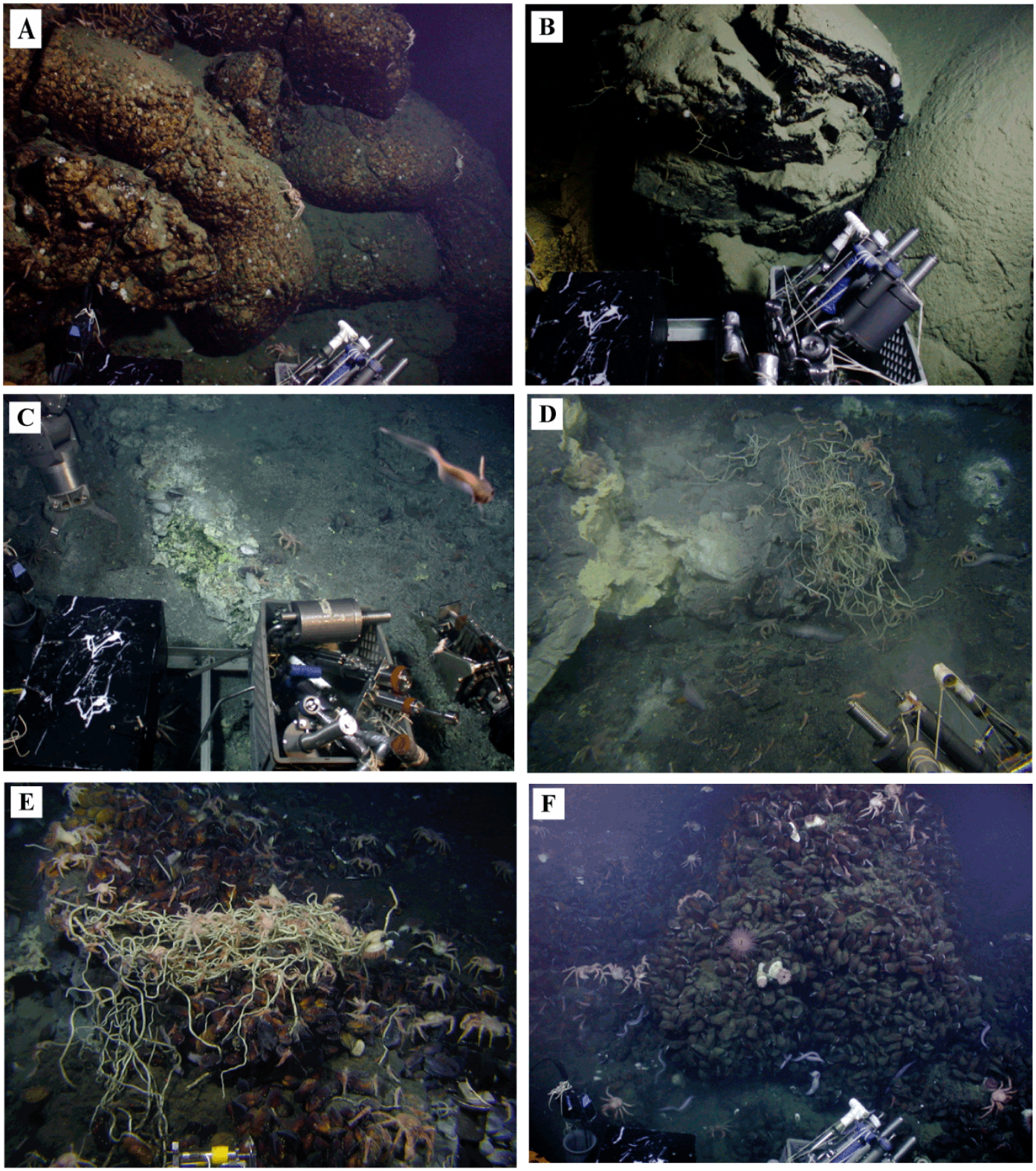

Figure 4. Leybourne et al

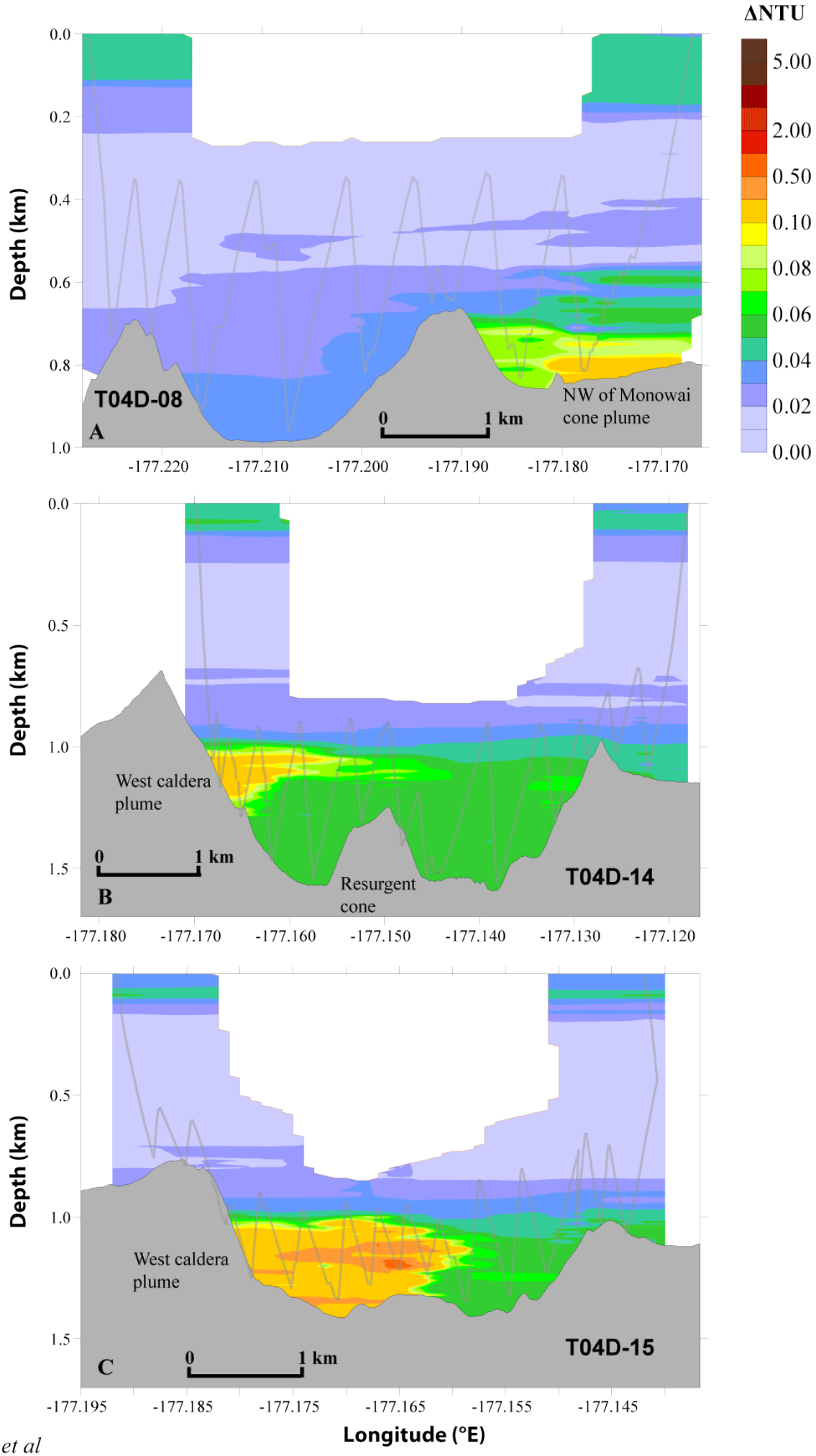

Figure 5. Leybourne et al

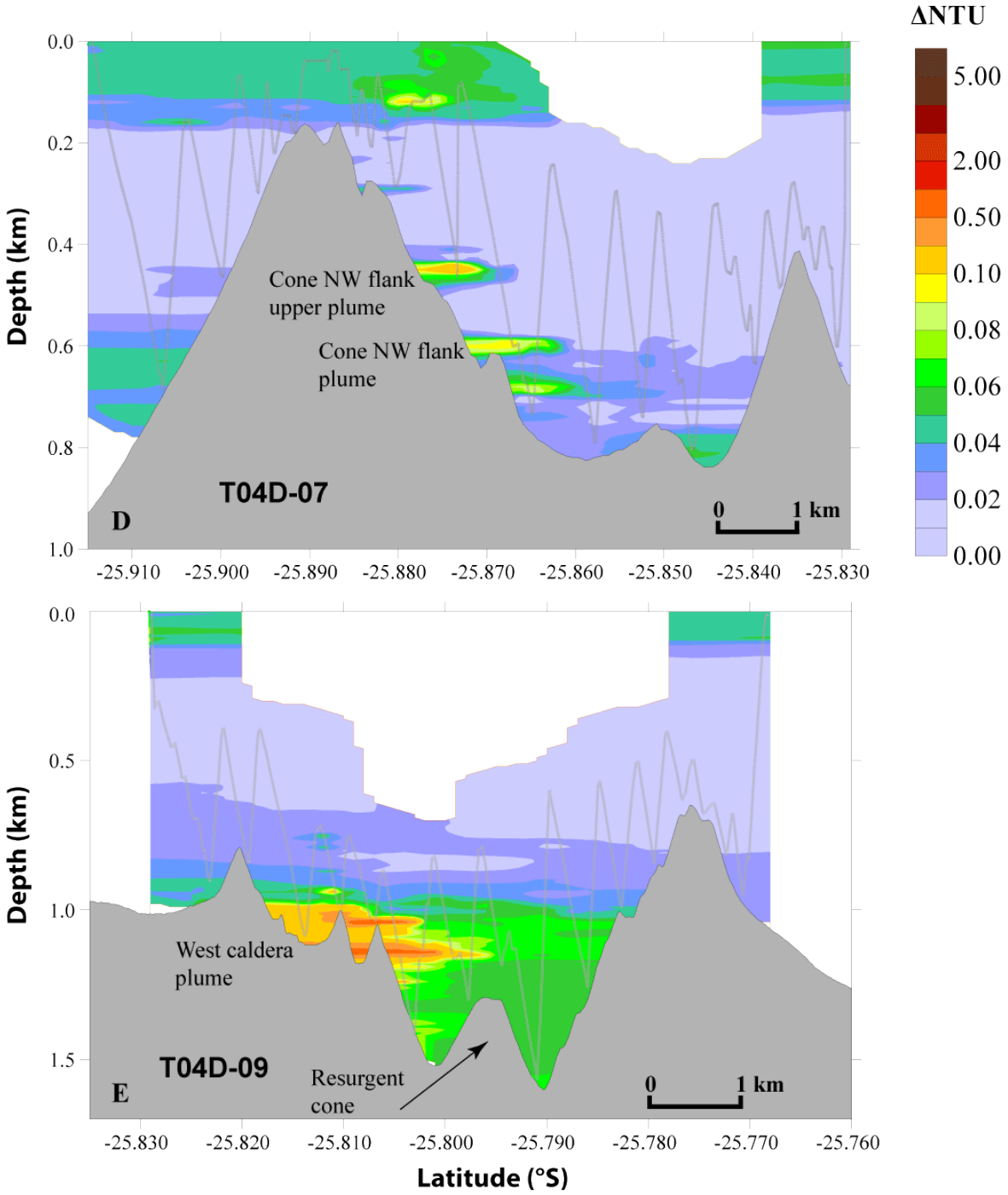

Figure 5 (cont.). Leybourne et al

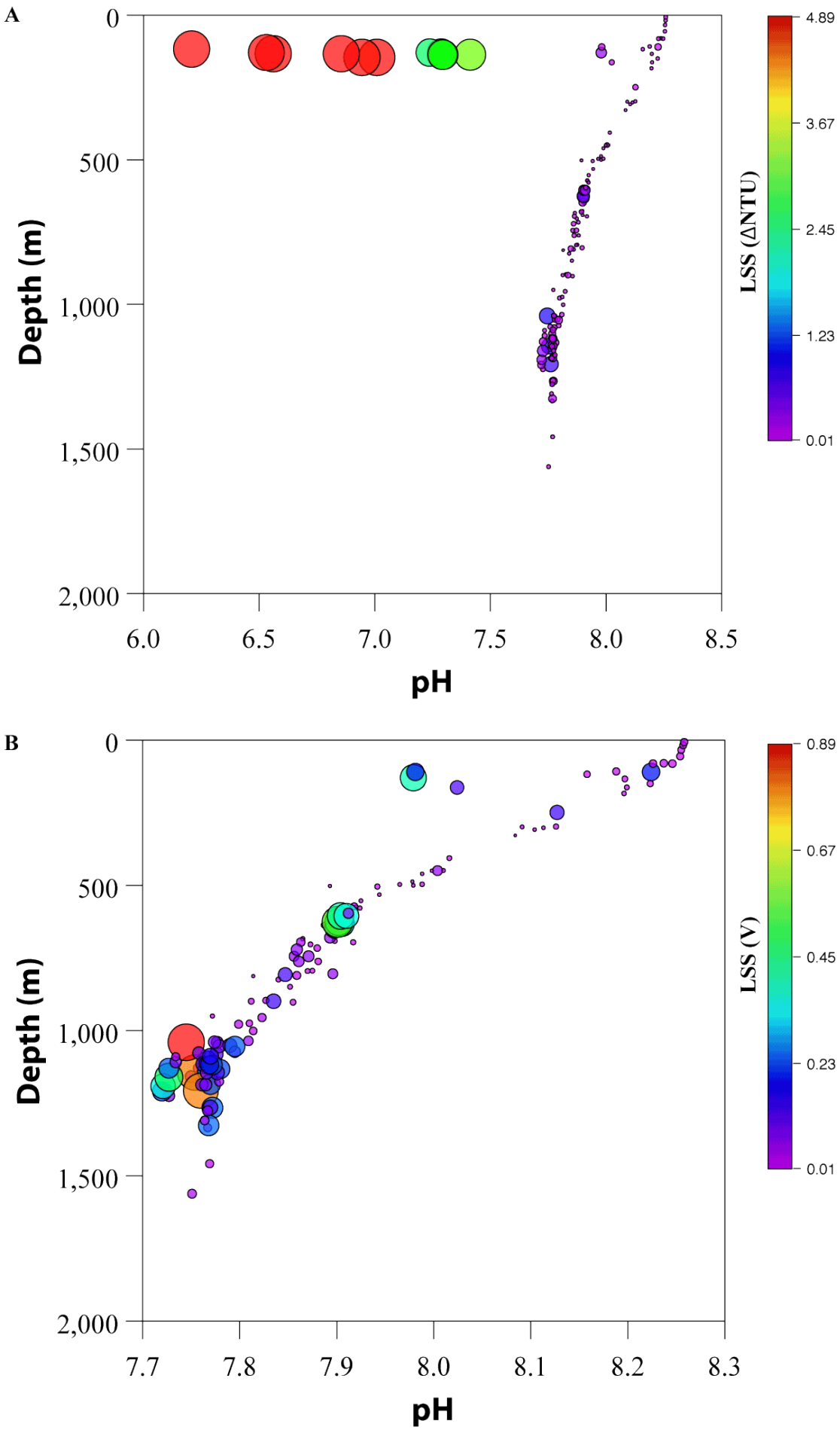

Figure 6. Leybourne et al

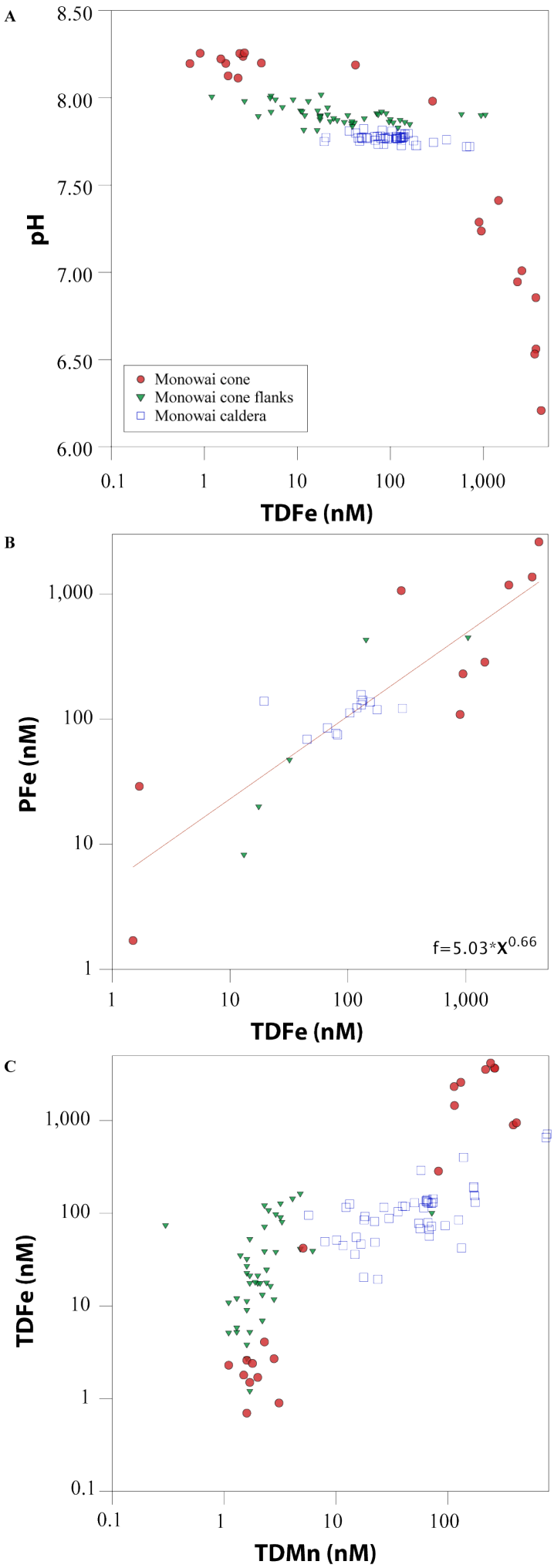

Figure 7. Leybourne et al

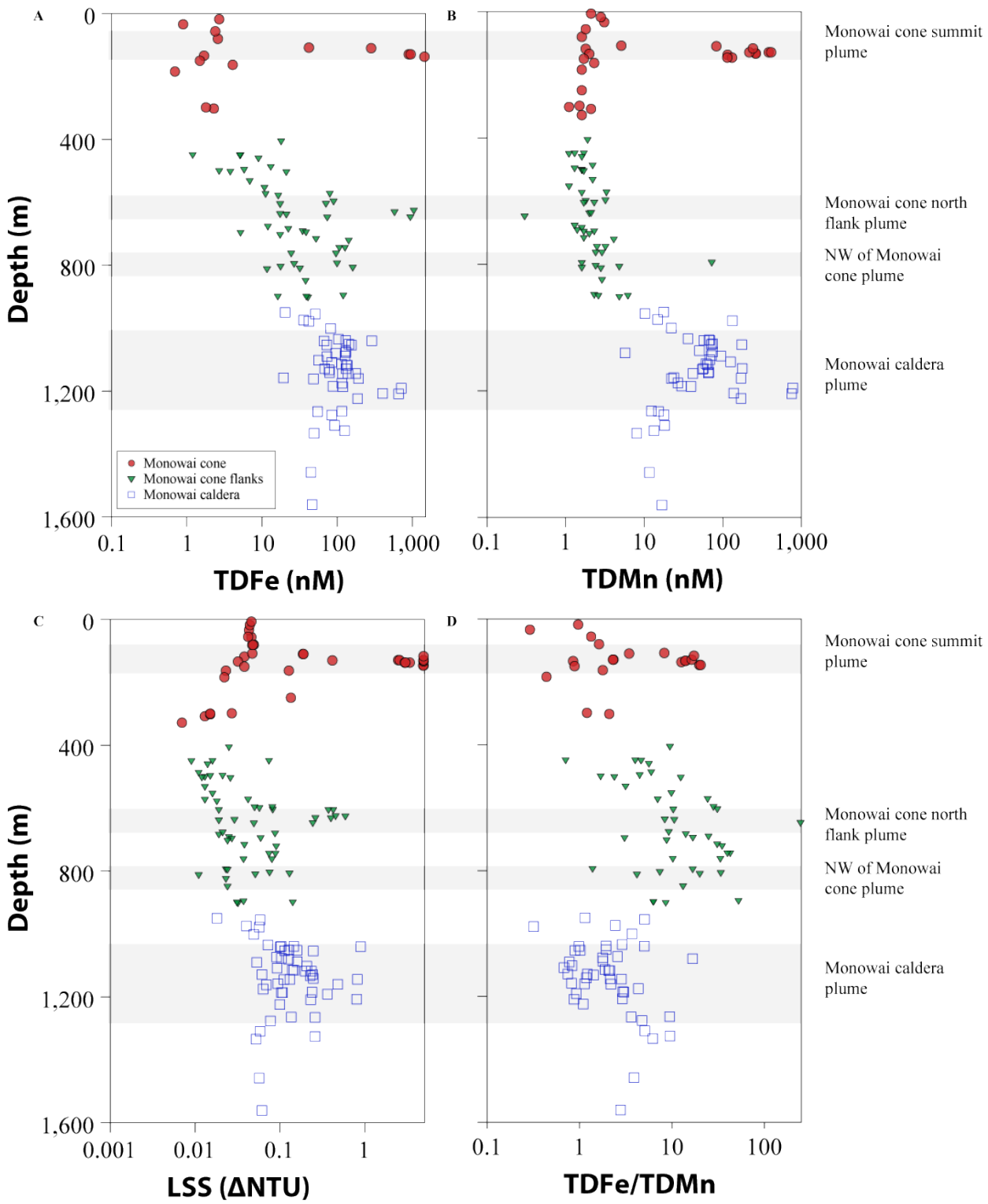

Figure 8. Leybourne et al

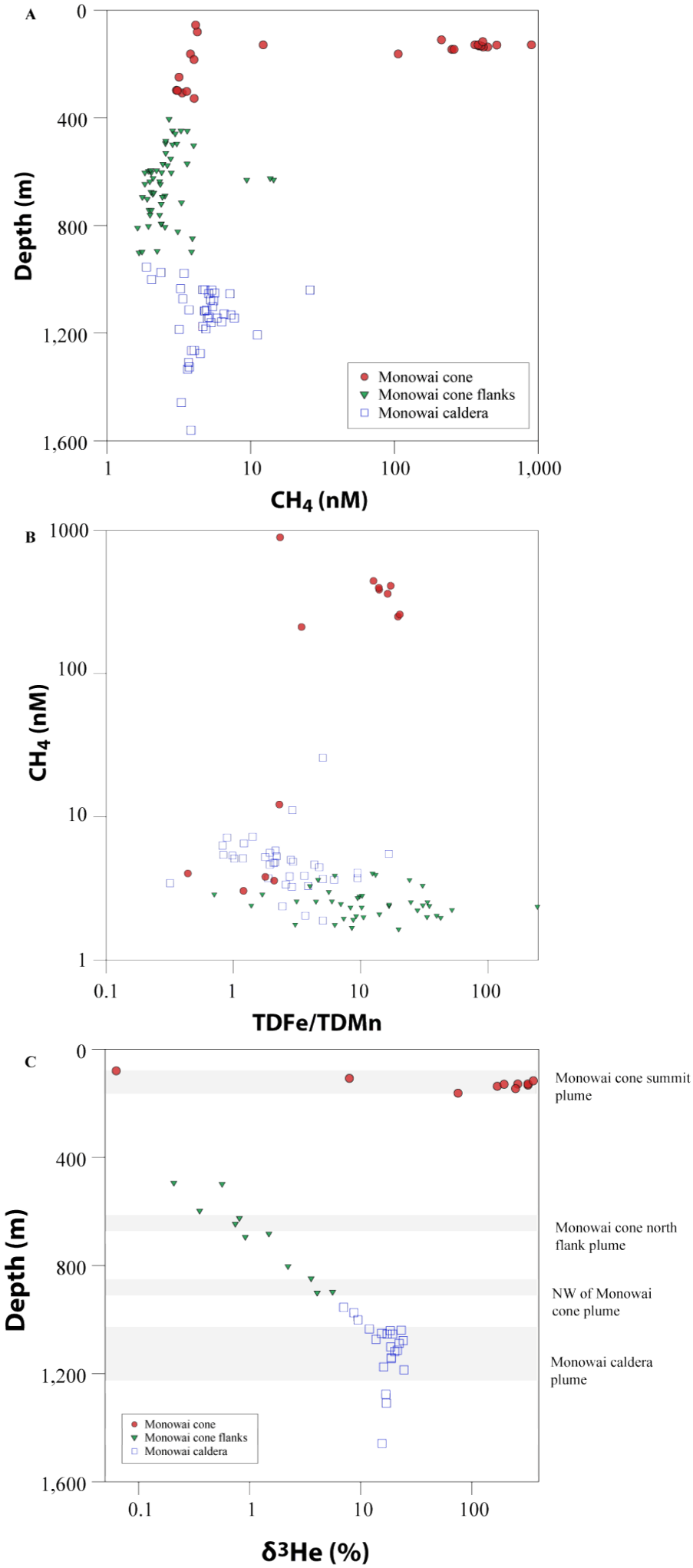

Figure 9. Leybourne et al

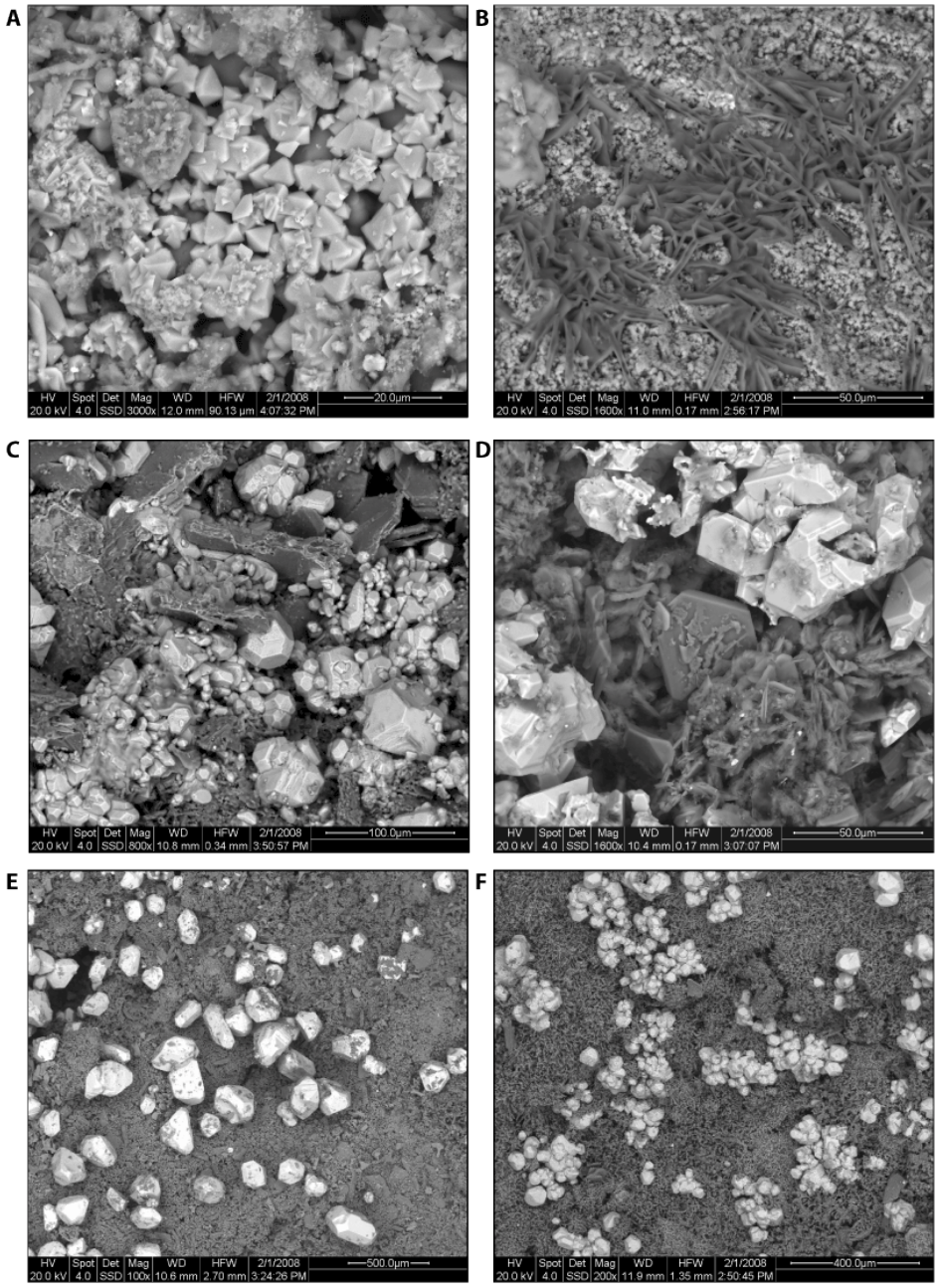

Figure 10. Leybourne et al

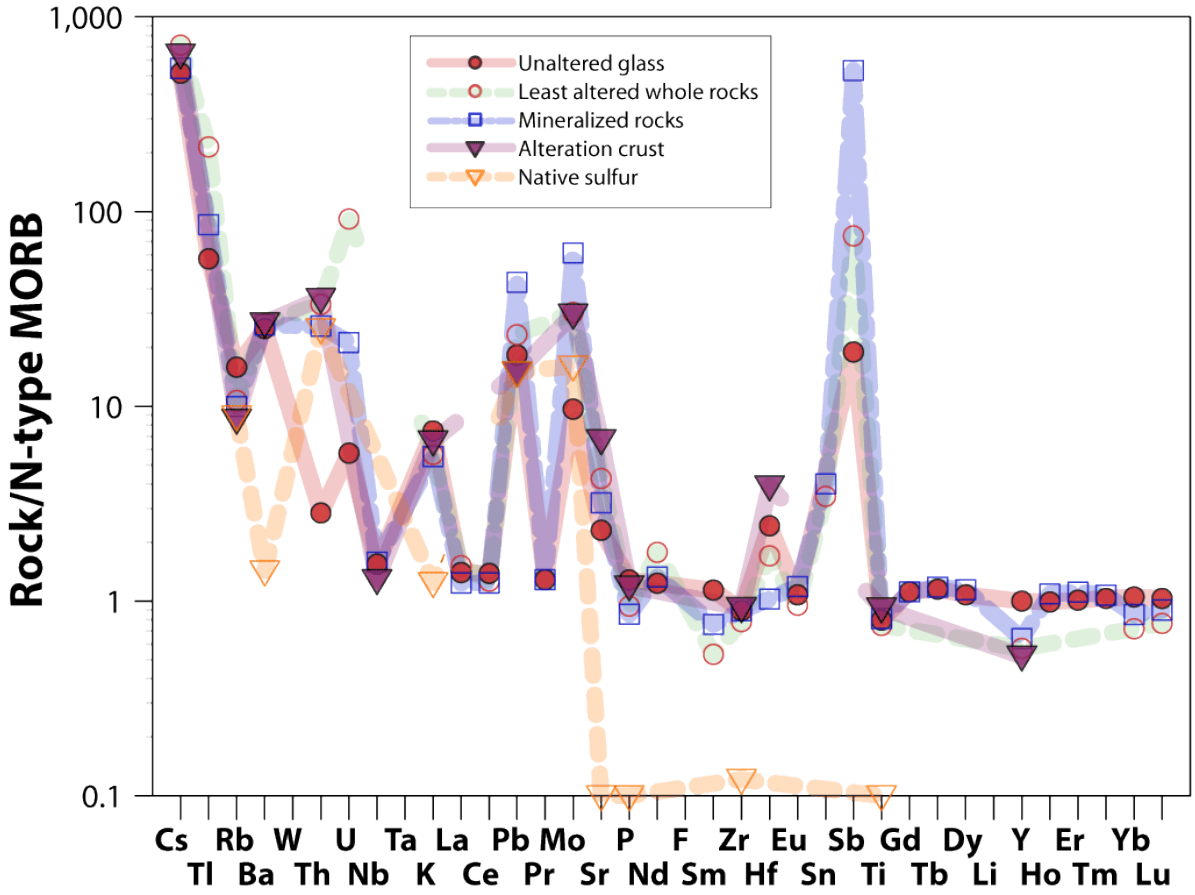

Figure 11. Leybourne et al

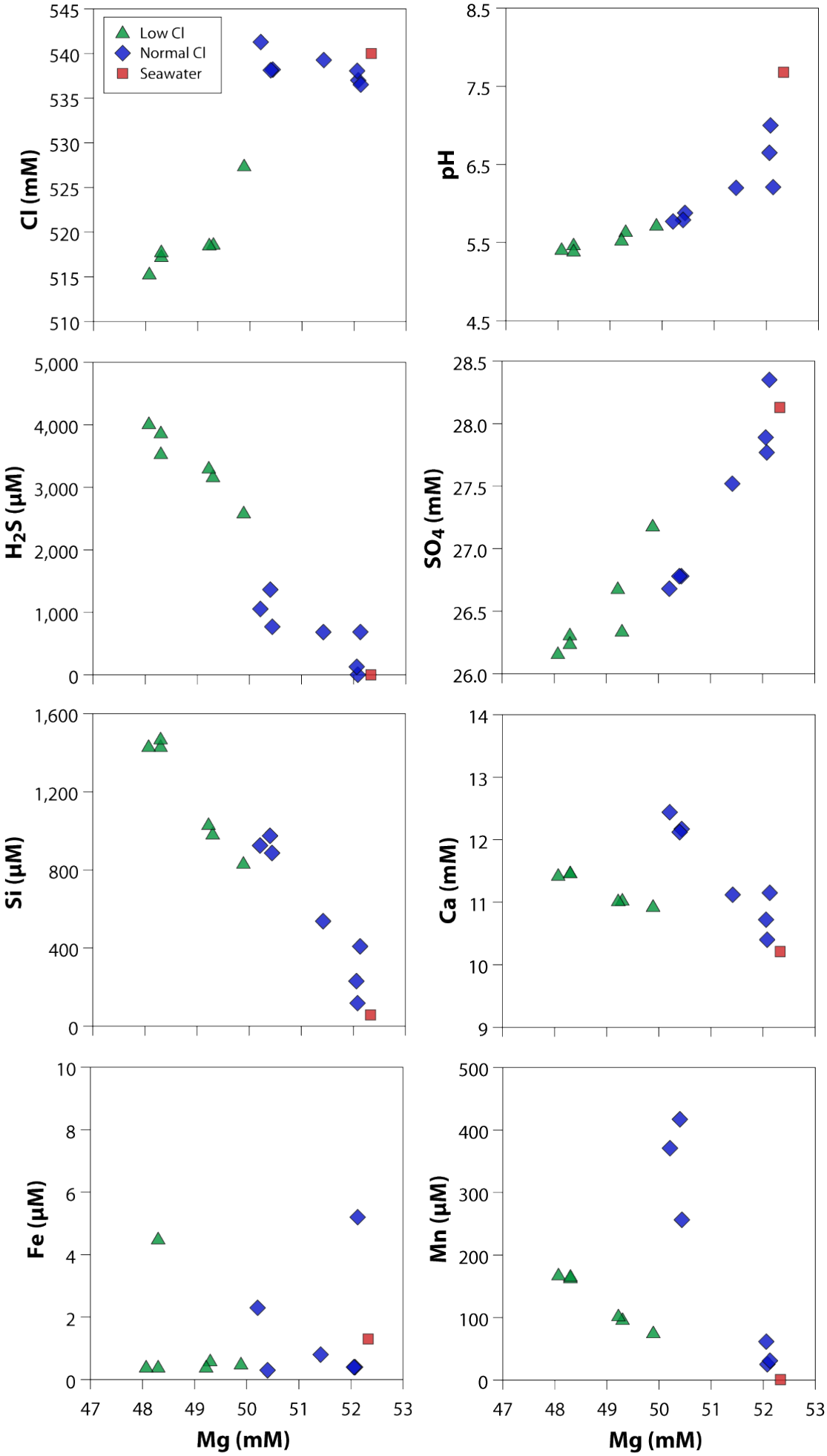

Figure 12. Leybourne et al

Table 1. Hydrothermal plume samples from tow-yos and vertical casts over Monowai cone and caldera

	Bottle Position	Nisken	Date	Time	Pressure	Depth m	Temp °C	Salinity PSU	θ	σ θ	LSS V
T04D-09	1	23	Sep 30 2004	23:10:54	831.0	824	5.90	34.37	5.82	27.08	0.023
NE-SW	2	10	Oct 01 2004	0:59:32	1576.6	1561	3.98	34.43	3.85	27.35	0.061
across	3	5	Oct 01 2004	1:07:43	1139.1	1129	4.12	34.42	4.03	27.32	0.061
caldera	4	4	Oct 01 2004	1:19:12	800.5	794	6.58	34.39	6.50	27.00	0.023
	5	28	Oct 01 2004	1:34:53	1169.1	1158	4.08	34.43	3.99	27.33	0.094
	6	6	Oct 01 2004	1:45:10	986.7	978	4.86	34.39	4.77	27.22	0.057
	7	1	Oct 01 2004	1:49:32	1154.5	1144	4.07	34.43	3.98	27.33	0.812
	9	17	Oct 01 2004	2:09:24	1049.6	1040	4.27	34.42	4.19	27.30	0.888
	11	9	Oct 01 2004	2:37:40	1089.5	1080	4.33	34.41	4.24	27.29	0.126
	12	12	Oct 01 2004	3:16:55	904.2	896	5.35	34.37	5.28	27.15	0.037
	13	13	Oct 01 2004	3:19:25	801.7	795	6.38	34.38	6.31	27.03	0.024
	14	14	Oct 01 2004	3:22:19	696.2	691	7.48	34.45	7.41	26.93	0.025
	15	15	Oct 01 2004	3:25:49	557.4	553	8.96	34.59	8.90	26.81	0.016
	16	16	Oct 01 2004	3:29:17	452.4	449	12.37	35.00	12.31	26.53	0.016
	17	8	Oct 01 2004	3:33:31	310.1	308	16.60	35.48	16.55	25.99	0.013
T04D-14	1	3	Oct 03 2004	6:33:14	1049.9	1040.5	4.29	34.41	4.21	27.30	0.100
NW-SE	3	28	Oct 03 2004	6:48:23	983.0	974.4	4.87	34.38	4.79	27.21	0.040
across	4	4	Oct 03 2004	6:50:52	1062.6	1053.1	4.30	34.41	4.22	27.30	0.113
caldera	5	17	Oct 03 2004	6:53:40	1151.1	1140.6	4.06	34.43	3.97	27.33	0.246
	6	6	Oct 03 2004	7:08:00	1111.6	1101.5	4.09	34.42	4.00	27.33	0.206
	7	22	Oct 03 2004	7:15:30	1472.4	1457.8	3.97	34.43	3.85	27.35	0.057
T04D-15	1	13	Oct 04 2004	9:18:19	1346.8	1334	4.01	34.43	3.90	27.34	0.052
parallel	2	25	Oct 04 2004	9:22:14	1171.9	1161	4.15	34.42	4.05	27.32	0.069
west	3	22	Oct 04 2004	9:28:57	1142.2	1132	4.21	34.42	4.12	27.31	0.226
caldera	4	4	Oct 04 2004	9:41:31	1218.2	1207	4.06	34.43	3.96	27.34	0.799
wall	5	28	Oct 04 2004	9:53:40	1276.8	1265	4.02	34.43	3.92	27.34	0.258
	7	5	Oct 04 2004	10:07:37	1338.9	1326	3.99	34.43	3.89	27.34	0.258
	9	21	Oct 04 2004	10:10:58	1276.4	1264	4.01	34.43	3.91	27.34	0.135
	11	1	Oct 04 2004	10:23:03	1196.0	1185	4.05	34.43	3.95	27.34	0.238
V04D-08	1	23	Oct 01 2004	6:12:20	1321.5	1309	3.97	34.43	3.87	27.35	0.058
Over	2	10	Oct 01 2004	6:14:41	1288.2	1276	3.97	34.43	3.87	27.35	0.077
central	3	5	Oct 01 2004	6:17:12	1185.9	1175	4.05	34.43	3.96	27.33	0.063
cone in	4	4	Oct 01 2004	6:20:37	1154.4	1144	4.11	34.42	4.02	27.33	0.131
caldera	5	3	Oct 01 2004	6:23:56	1060.6	1051	4.31	34.41	4.23	27.29	0.127
	6	6	Oct 01 2004	6:24:09	1061.3	1052	4.31	34.41	4.23	27.29	0.158
	7	22	Oct 01 2004	6:28:29	856.7	849	5.61	34.36	5.53	27.11	0.024
	9	7	Oct 01 2004	6:31:46	689.2	684	7.11	34.42	7.04	26.96	0.019
	11	9	Oct 01 2004	6:36:01	504.3	500	10.92	34.82	10.86	26.66	0.013
	12	12	Oct 01 2004	6:39:52	304.4	302	16.53	35.48	16.48	26.00	0.015
V04D-12	1	15	Oct 03 2004	11:30:28	1082.7	1073	4.39	34.41	4.30	27.28	0.091
Over	3	28	Oct 03 2004	11:32:54	1063.2	1054	4.45	34.40	4.36	27.27	0.245
Mussel	5	26	Oct 03 2004	11:35:09	1044.1	1035	4.52	34.40	4.43	27.26	0.072
Ridge	7	9	Oct 03 2004	11:37:30	1010.1	1001	4.58	34.40	4.50	27.25	0.049
west	9	7	Oct 03 2004	11:45:32	909.3	902	5.45	34.36	5.38	27.13	0.032
caldera	11	1	Oct 03 2004	11:49:44	701.4	696	7.25	34.43	7.18	26.94	0.027
	12	12	Oct 03 2004	11:53:49	499.4	496	11.09	34.85	11.03	26.65	0.021
	13	13	Oct 03 2004	11:57:42	300.2	298	16.87	35.51	16.82	25.95	0.027
V04D-13	1	22	Oct 03 2004	19:51:07	1086.6	1077	4.15	34.42	4.07	27.32	0.104
NW	2	25	Oct 03 2004	20:06:21	1124.8	1115	4.06	34.43	3.97	27.33	0.146
caldera	3	3	Oct 03 2004	20:06:51	1124.5	1114	4.06	34.43	3.97	27.33	0.139
wall	4	4	Oct 03 2004	20:17:25	1197.2	1186	4.02	34.43	3.92	27.34	0.107
	5	17	Oct 03 2004	20:17:59	1197.6	1186	4.02	34.43	3.93	27.34	0.104
	6	6	Oct 03 2004	20:20:05	1155.9	1145	4.02	34.43	3.93	27.34	0.111
	7	5	Oct 03 2004	20:21:41	1127.8	1118	4.06	34.43	3.97	27.33	0.233
	9	7	Oct 03 2004	20:22:53	1128.2	1118	4.06	34.43	3.98	27.33	0.198
	11	1	Oct 03 2004	20:25:22	1097.7	1088	4.12	34.42	4.03	27.32	0.159
	12	12	Oct 03 2004	20:29:10	1048.6	1039	4.25	34.42	4.17	27.30	0.145
	13	13	Oct 03 2004	20:29:50	1048.8	1039	4.25	34.42	4.17	27.30	0.103
	14	2	Oct 03 2004	20:33:08	963.6	955	5.04	34.38	4.96	27.19	0.058
	15	23	Oct 03 2004	20:35:00	907.1	899	5.30	34.37	5.23	27.15	0.141
	16	16	Oct 03 2004	20:38:23	810.7	804	6.19	34.38	6.11	27.05	0.075
	17	11	Oct 03 2004	20:42:37	604.2	599	8.08	34.50	8.02	26.88	0.057
	18	18	Oct 03 2004	20:46:00	452.2	449	12.29	34.99	12.23	26.53	0.074
	19	19	Oct 03 2004	20:50:38	250.4	249	17.61	35.55	17.56	25.80	0.134
V05A-01	1	3	Apr 08 2005	20:01:30	1235.4	1224	3.97	34.39	3.87	27.31	0.099
	4	25	Apr 08 2005	20:06:57	1220.8	1209	3.99	34.39	3.90	27.31	0.230
	6	10	Apr 08 2005	20:10:09	1201.7	1191	4.00	34.39	3.91	27.31	0.361
	7	15	Apr 08 2005	20:13:08	1170.4	1160	4.04	34.38	3.95	27.30	0.477
	9	8	Apr 08 2005	20:16:12	1139.4	1129	4.09	34.38	4.00	27.29	0.241
	12	12	Apr 08 2005	20:19:15	1118.0	1108	4.14	34.37	4.06	27.28	0.092
	13	28	Apr 08 2005	20:21:49	1100.2	1090	4.17	34.37	4.08	27.28	0.053
	15	26	Apr 08 2005	20:27:22	957.9	950	4.82	34.32	4.74	27.17	0.018
	17	19	Apr 08 2005	20:31:49	819.0	812	5.72	34.31	5.65	27.05	0.011
	19	11	Apr 08 2005	20:38:57	505.7	502	9.35	34.59	9.29	26.75	0.012
	21	13	Apr 08 2005	20:47:54	119.3	118	19.53	35.59	19.51	25.34	0.038
T04D-07	1	24	Sep 30 2004	6:50:02	609.9	605	8.05	34.50	7.99	26.89	0.019
N-S	2	2	Sep 30 2004	6:53:35	453.9	450	12.71	35.04	12.65	26.49	0.009

Table 1. Hydrothermal plume samples from tow-yos and vertical casts over Monowai cone and caldera

over lesser	3	11	Sep 30 2004	7:07:51	490.2	487	11.73	34.92	11.67	26.59	0.011
and greater	4	4	Sep 30 2004	7:17:57	642.9	638	8.10	34.51	8.03	26.88	0.019
cones	5	28	Sep 30 2004	7:23:26	578.0	573	9.01	34.60	8.95	26.81	0.013
	6	6	Sep 30 2004	7:27:41	463.5	460	12.10	34.97	12.04	26.56	0.014
	7	1	Sep 30 2004	7:30:44	330.6	328	15.66	35.36	15.60	26.12	0.007
	9	3	Sep 30 2004	7:39:50	816.8	810	6.02	34.37	5.95	27.06	0.051
	11	17	Sep 30 2004	7:43:41	682.4	677	7.42	34.45	7.35	26.93	0.021
	12	12	Sep 30 2004	8:37:02	685.3	680	7.26	34.44	7.20	26.95	0.087
	13	15	Sep 30 2004	8:39:32	609.3	604	8.13	34.51	8.06	26.88	0.082
	14	14	Sep 30 2004	9:24:28	164.0	163	19.51	35.68	19.48	25.42	0.023
	15	23	Sep 30 2004	9:26:19	134.6	134	20.16	35.67	20.13	25.24	0.032
	16	16	Sep 30 2004	9:51:24	185.5	184	19.46	35.68	19.43	25.43	0.022
	17	8	Sep 30 2004	9:53:12	151.3	150	19.66	35.72	19.64	25.40	0.038
T04D-08	1	23	Sep 30 2004	16:30:43	906.7	899	5.52	34.37	5.44	27.12	0.031
NW-SE	2	10	Sep 30 2004	16:35:00	708.3	703	7.19	34.43	7.12	26.96	0.024
Between	3	5	Sep 30 2004	16:47:54	507.6	504	10.50	34.77	10.43	26.69	0.026
cone and	4	4	Sep 30 2004	17:20:40	768.6	762	7.28	34.44	7.21	26.95	0.037
caldera	5	28	Sep 30 2004	17:41:47	642.5	637	7.57	34.46	7.51	26.93	0.029
over small	6	6	Sep 30 2004	17:55:35	700.9	695	6.51	34.39	6.45	27.01	0.059
east cone	7	1	Sep 30 2004	17:58:43	749.8	744	6.27	34.37	6.20	27.03	0.074
	9	7	Sep 30 2004	18:05:17	726.7	721	6.35	34.37	6.28	27.02	0.090
	11	9	Sep 30 2004	18:24:15	813.5	807	5.99	34.36	5.92	27.06	0.129
	12	12	Sep 30 2004	18:26:57	768.2	762	6.36	34.38	6.29	27.02	0.080
	13	13	Sep 30 2004	18:29:23	749.7	744	6.66	34.39	6.59	26.99	0.088
	14	14	Sep 30 2004	18:31:06	722.3	716	6.88	34.40	6.81	26.97	0.038
	15	15	Sep 30 2004	18:34:40	653.4	648	8.26	34.52	8.19	26.87	0.049
	16	16	Sep 30 2004	18:36:39	601.5	597	8.54	34.55	8.48	26.85	0.050
	17	8	Sep 30 2004	18:38:38	576.8	572	9.09	34.60	9.02	26.80	0.042
	18	18	Sep 30 2004	18:41:10	536.4	532	10.43	34.75	10.36	26.70	0.013
	19	19	Sep 30 2004	18:45:14	409.2	406	13.14	35.10	13.08	26.45	0.025
V04D-07	1	22	Sep 30 2004	13:17:37	129.8	129	19.80	35.68	19.78	25.34	2.459
Over	2	2	Sep 30 2004	13:18:02	129.9	129	19.80	35.68	19.78	25.34	2.545
Main	3	5	Sep 30 2004	13:19:43	109.0	108	20.17	35.68	20.15	25.24	0.047
Cone	5	28	Sep 30 2004	13:21:43	80.2	80	20.89	35.62	20.87	25.00	0.049
	7	1	Sep 30 2004	13:24:24	56.3	56	21.21	35.52	21.20	24.83	0.046
	11	9	Sep 30 2004	13:26:36	34.2	34	21.22	35.49	21.22	24.81	0.043
	13	13	Sep 30 2004	13:28:21	18.3	18	21.22	35.49	21.22	24.81	0.044
	15	15	Sep 30 2004	13:29:57	7.4	7	21.23	35.49	21.23	24.81	0.046
V04D-14	1	22	Oct 04 2004	0:50:53	138.3	137	19.91	35.69	19.88	25.32	3.354
Over	2	25	Oct 04 2004	0:51:22	138.2	137	19.91	35.69	19.88	25.32	2.942
Main	3	3	Oct 04 2004	0:51:53	138.3	137	19.93	35.69	19.91	25.31	2.989
Cone	4	4	Oct 04 2004	0:52:43	130.9	130	19.98	35.67	19.96	25.29	0.413
	5	26	Oct 04 2004	0:55:35	111.2	110	20.28	35.67	20.26	25.20	0.186
	6	6	Oct 04 2004	0:55:47	111.2	110	20.28	35.67	20.26	25.20	0.188
	7	5	Oct 04 2004	0:58:30	81.5	81	20.98	35.63	20.96	24.99	0.047
	9	28	Oct 04 2004	0:58:59	81.5	81	20.97	35.63	20.95	24.99	0.048
	11	1	Oct 04 2004	1:01:12	55.3	55	21.24	35.54	21.23	24.85	0.042
V04D-15	1	13	Oct 04 2004	3:57:56	164.3	163	19.38	35.73	19.35	25.49	0.127
Over	2	25	Oct 04 2004	3:59:17	146.5	146	19.73	35.70	19.70	25.38	4.894
Main	3	3	Oct 04 2004	3:59:42	146.6	146	19.71	35.70	19.69	25.38	4.849
Cone	4	4	Oct 04 2004	4:01:25	134.0	133	19.92	35.69	19.89	25.32	4.894
	5	15	Oct 04 2004	4:01:36	133.9	133	19.90	35.69	19.88	25.32	4.894
	6	6	Oct 04 2004	4:04:23	129.9	129	19.89	35.69	19.87	25.32	4.894
	7	5	Oct 04 2004	4:04:35	130.2	129	19.86	35.69	19.83	25.33	4.894
	9	28	Oct 04 2004	4:06:29	117.7	117	19.86	35.69	19.84	25.33	4.894
V04D-16	1	13	Oct 04 2004	6:34:57	636.4	631	7.89	34.49	7.83	26.90	0.260
On North	2	25	Oct 04 2004	6:35:30	637.4	632	7.85	34.48	7.78	26.90	0.397
Flank	3	22	Oct 04 2004	6:37:15	652.4	647	7.45	34.45	7.39	26.93	0.242
of main	4	4	Oct 04 2004	6:38:22	630.3	625	8.06	34.50	7.99	26.88	0.449
Cone	5	26	Oct 04 2004	6:38:36	630.6	626	8.07	34.50	8.00	26.88	0.587
	6	6	Oct 04 2004	6:40:26	610.2	605	8.19	34.51	8.13	26.87	0.423
	7	5	Oct 04 2004	6:40:43	610.1	605	8.20	34.51	8.14	26.87	0.371
	9	21	Oct 04 2004	6:41:55	601.0	596	8.37	34.53	8.30	26.86	0.081
	11	1	Oct 04 2004	6:43:16	582.9	578	8.93	34.59	8.86	26.82	0.018
	12	12	Oct 04 2004	6:45:09	501.3	497	11.03	34.84	10.97	26.66	0.015
	13	17	Oct 04 2004	6:49:52	301.6	299	16.27	35.45	16.22	26.04	0.015

pH	TDFe nM	TDMn nM	DFe nM	DMn nM	TDFe/TDMn	CH_4 nM	Corr[3]He E-14	Corr[4]He E-8	δ^3He %	H_2S µM	DFe/TDFe	DMn/TDMn
7.840						3.12						
7.751	46.5	16.8			2.8	3.85						
7.757	68.5	56.6			1.2	6.54						
7.875	99.7	72.2			1.4	2.40						
7.750	19.4	23.7			0.8	6.31						
7.799	42.2	133.1			0.3	3.45						
7.754	177.0					7.71						
7.745	290.0	57.6			5.0	25.89						
7.776	95.2	5.7			16.7	5.54						
7.827	120.5	2.3			52.4	2.24						
7.870	26.8	1.6			16.8	2.39						
7.898	34.8	1.4			24.9	2.54						
7.925	10.8	1.1			9.8	2.78						
8.010	5.2	1.3			4.0	3.28						
8.104	0.0	2.1			0.0	3.35						
7.777	67.0	68.3	27.7	66.6	1.0	5.37	6.900	4.178	18.520		0.41	0.98
7.810	36.0	14.8			2.4	2.38	6.168	4.083	8.680			
7.779	72.6	71.6			1.0	5.12	6.765	4.150	17.290			
7.767	79.1	66.6	29.7	64.4	1.2	5.15	6.900	4.175	18.900		0.38	0.97
7.767	56.7	68.3			0.8	5.44	6.917	4.196	18.590			
7.769	44.9	11.6	7.9	10.9	3.9	3.30	6.605	4.112	15.580		0.18	0.94
7.767	49.6	8.0			6.2	3.65						
7.773	48.6	22.3			2.2	5.31						
7.780	77.9	55.0			1.4	7.29						
7.760	401.0	138.0			2.9	11.16						
7.772	55.0	15.2			3.6	3.89						
7.768	126.0	13.3			9.5	3.75						
7.770	116.0	12.3			9.4	4.06						
7.770	87.9	29.9			2.9	4.88						
7.764	92.3	18.2			5.1	3.70						
7.767	84.8	17.9			4.7	4.47						
7.779	115.8	26.8			4.3	4.66						
7.777	139.8	65.3			2.1	5.85						
7.790	143.5	74.1			1.9	5.63						
7.852	38.1	2.9			13.1	3.94						
7.865	22.5	1.6			14.1	2.09						
7.979	2.7	1.6			1.7	2.87						
8.113	2.3	1.1			2.1	3.60						
7.795	130.0	50.4	10.9	42.4	2.6	3.38					0.08	0.84
7.795	154.9	174.0	42.3	92.5	0.9	7.20					0.27	0.53
7.809	103.8	36.0	8.4	27.9	2.9	3.26					0.08	0.78
7.814	81.6	22.2	5.4	14.7	3.7	2.05					0.07	0.66
7.855	41.0	4.8			8.5	1.68						
7.917	5.2	1.7			3.1	1.77						
7.988	5.8	1.3			4.5	2.56						
8.126	1.8	1.5			1.2	3.05						
7.758	131.3	73.8			1.8	5.26						
7.763						4.95						
7.766	114.7	61.0			1.9	3.73						
7.761						3.19						
7.765	119.1	39.4	27.2	37.5	3.0						0.23	0.95
7.766	118.0	41.6			2.8	5.03						
7.772	136.2	64.2			2.1	4.82						
7.769	133.5	64.4	16.8	57.8	2.1	4.78					0.13	0.90
7.770	127.5	71.6			1.8							
						4.81						
7.774	129.7	67.0	16.5	70.2	1.9	4.66					0.13	1.05
7.823	51.5	10.2			5.0	1.89						
7.835	38.9	6.2			6.3	1.76						
7.896	17.7	2.4			7.4	1.95						
		1.8				1.95						
8.004	1.2	1.7			0.7	2.87						
8.127		1.6				3.18						
7.727	187.0	171.0			1.1							
7.720	657.0	755.0			0.9							
7.721	713.0	775.0			0.9							
7.727	193.0	171.0			1.1							
7.727	131.0	176.0			0.7							
7.734	84.8	125.5			0.7							
7.734	73.5	94.8			0.8							
7.772	20.3	17.7			1.1							
7.814	11.7	2.8			4.2							
7.893	3.8	1.6			2.4							
8.158		1.8										
7.895	17.5	1.7			10.3	2.81						
7.998	5.1	1.1			4.6	3.63						

7.978	13.1	2.2			6.0	2.57						
7.902	21.1	2.0			10.6	1.99						
7.920	11.2	1.6			7.0	2.46						
7.988	9.0	1.6			5.6	2.99						
8.084	-0.4	1.6			-0.3	4.05						
7.859	31.9	1.6			19.9	1.64						
7.897	12.0	1.3			9.2	2.03						
7.893						2.12						
7.909	71.1	2.3			30.9	2.41						
8.199	4.1	2.3			1.8	3.82						
8.197	1.7	2.0			0.9							
8.196	0.7	1.6			0.4	4.04						
8.223	1.5	1.7			0.9							
7.812	16.3	2.6			6.3	3.89						
7.873	17.5	2.0			8.8	1.91						
7.942	21.1	1.7			12.4	4.02						
7.881	24.5	2.4			10.2	2.33						
7.887	17.5	2.1			8.3	2.33						
7.863	38.6	2.3			16.8	2.44						
7.856	106.8	2.5			42.7	1.97						
7.859	142.5	4.1	7.7	1.8	34.8	2.39					0.05	0.44
7.847	161.3	4.8			33.6	2.54						
7.861	96.7	2.9			33.3	2.00						
7.871	126.9	3.2			39.7	2.04						
7.880	52.3	1.7			30.8	3.31						
7.903	73.8	0.3			246.0	2.36						
7.909	89.8	3.2			28.1	2.22						
7.918	80.1	3.3			24.3	3.62						
7.944	6.9	2.2			3.1	2.57						
8.016	18.0	1.9			9.5	2.71						
7.288	896.0	385.0	725	419	2.3	895.34				27.3	0.81	1.09
7.237	947.0	412.0			2.3	12.23				32.8		
8.188	42.1	5.1			8.3		0.000	0.000	7.920			
8.237	2.6	1.6			1.6							
8.254	2.4	1.8			1.3							
8.255	0.9	3.1			0.3							
8.257	2.7	2.8			1.0							
8.258		2.1										
7.412	1452.0	115.0	526	98	12.6	444.77				2.2	0.36	0.85
7.296						413.27						
7.293												
7.979						513.90				7.4		
7.981	284.0	82.7	5.1	84.5	3.4	212.01					0.02	1.02
8.224												
8.226												
8.246						4.26						
						4.15						
8.024				72.3		106.29						
7.009	2583.0	131.0			19.7	250.30				14.4		
6.945	2320.0	114.0		127	20.4	259.20				12.7		1.11
6.561	3670.0	262.0			14.0	386.50				22.5		
6.855	3660.0	263.0	2289	285	13.9	398.77				25.1	0.63	1.08
6.531	3555.0	218.0			16.3	361.96				10		
						381.90						
6.208	4178.0	242.0	2202	241	17.3	411.04				5.2	0.53	1.00
7.905	580.0					14.45						
7.905						9.40						
7.898	941.0					1.84						
7.902						2.10						
7.901	1046.0					13.67						
7.904						2.04						
7.910						1.84						
7.912						2.02						
7.924	16.5					2.64						
7.965						3.07						
8.091						3.10						

Sampling and analytical methods

All tows and casts used a high-precision SeaBird 911plus CTDO equipped with conductivity, temperature and pressure (depth) and optical light scattering sensors. The temperature and conductivity sensors have accuracies of better than ± 0.001°C and ± 0.0003 S/m, respectively. The light-scattering sensor (LSS; Seapoint Sensors) detects back-scattered light from two modulated 880-nm light-emitting diodes, with a resolution of ± 0.0005 V (0.01% full scale). Sensors were monitored in real-time by graphic and analogue output displayed on a computer monitor. The water sampling bottles were maintained 'trace metal clean' by Teflon coating all wet surfaces and using non-contaminating materials for O-rings, springs, and spigots with the water sampling rosette configured to hold the Niskin bottles and the CTDO instrumentation. Discrete water samples were collected in custom-built 19 L PVC bottles attached to the towable profiling package. The bottles were closed using silastic springs actuated by remote control shipboard in real-time. The first aliquot taken from the Niskin bottles was for helium isotope determination, to prevent contamination by atmospheric helium. Helium samples were stored in 25 cm long sections of Cu refrigeration tubing cold-welded at both ends to insure sample integrity. Sub-samples for total dissolvable metals (TDMe), dissolved metals (DMe), and suspended particulate matter (SPM) were collected on-deck, directly from the Niskin samplers, into acid-cleaned high density polyethylene (HDPE) bottles via a shielded transfer tube. Metal samples were acidified to pH 1.9 using ultra-clean HCl. DMe, SPM, and SEM samples were obtained by vacuum filtration through acid-cleaned and pre-weighed 37 mm diameter, 0.4 µm pore size polycarbonate membranes.

Measurements of pH were made within an hour of retrieval of the CTDO on deck. Aliquots for pH were transferred by plastic tube from the Niskin bottles to the bottom of a 60 ml plastic bottle, overfilled to three-times capacity, and capped with no void space to

ensure no entrapment of air. An Orion Ross SureFlow combination hydrogen ion selective electrode and an Orion (model 250) pH meter were used to determine pH. The pH electrodes were standardized daily and all samples were thermally equilibrated in a recirculating bath for 30 minutes prior to analysis, with temperature compensation following pH measurements. All pH measurements are recalculated to account for the effects of salinity on the activity of H^+ (for seawater, typically the difference is 0.114 ± 0.013 pH units (Bates and Culberson, 1977; Gieskes et al., 1991). Measurements of pH performed in this manner have replicate precision of ± 0.001 pH units within a single cast or tow-yo, and a daily precision of around ± 0.005 pH units (Resing et al., 1999; Resing et al., 2004).

Total dissolvable Fe and Mn were measured by flow-injection analysis at GNS Science. TDFe was determined using the method of Measures et al. (1995), which involves reaction of Fe with N,N-dimethyl-*p*-phenylenediamine dihydrochloride with colorimetric detection. TDMn was also determined colorimetrically, using a modification of the leuco-malachite green method of Resing and Mottl (1992).

For on-board gas chromatography-based CH_4 analyses, 100 ml of seawater was collected in 140 ml syringes directly from the Niskin bottles after the rosette was brought onboard. The syringes were placed in a water bath for at least 30 min to equilibrate the samples to ambient temperature. Forty ml of high grade N_2 was then added to the 100 ml of seawater and vigorously agitated for 2 minutes to reach equilibrium between the CH_4 concentration in the water and in the gas phase. Experiments undertaken onboard and onshore have determined that this method has an extraction efficiency of 88% for a 100:40 H_2O:N_2 mixture. Measured CH_4 concentrations were corrected for extraction efficiency. Methane concentrations are also corrected for temperature and atmospheric pressure at the time of measurement. The lower limit of determination for dissolved CH_4 is ~ 0.5 nM and analytical precision is ~ 5%. Helium isotopes were determined using a 21-cm radius, dual collector mass spectrometer; the 1σ

precision for the $^3He/^4He$ measurements is 0.2% in δ^3He (Lupton et al., 1977). Helium enriched in ^3He enters seawater via hydrothermal circulation and is a definitive indicator of contributions from the mantle, either from magmatic volatiles or leaching of mafic volcanic rocks (e.g., Lupton et al., 1977). ^3He anomalies are measured in the water column over seafloor venting sites and are the single-most analytically sensitive and unequivocal tracer of sea floor hydrothermal activity. Thus, the detection of ^3He in plumes above Monowai cone and caldera is an important tracer of magmatic sources and hydrothermal circulation. These anomalies, however, represent small amounts of the original source fluid diluted with large amounts of ambient seawater. This dilution reduces the original $^3He/^4He$ value in the source fluids to a small percentage deviation expressed as a δ^3He value, where δ^3He (%) = $100\cdot[(R/R_A)-1]$. For samples highly enriched in helium (e.g., volcanic rocks and vent fluids) the helium isotope ratios are typically expressed as R/R_A, where $R = {}^3He/^4He$ and $R_A = (^3He/^4He)_{Air} = 1.4\cdot10^{-6}$.

Sampling of hydrothermal precipitates was carried out during MANGO 192-2 *ROPOS* cruise on the R/V *Sonne*. The composition of altered and mineralized basalts and basaltic andesites (n=43), alteration crusts (n=5), and sulphur precipitates (n=3) was determined by X-ray fluorescence spectrometry (XRF) on fused disks at the Bundesanstalt für Geowissenschaften und Rohstoffe (BGR), Hannover, and by inductively coupled plasma mass spectrometry at BGR and at Actlabs, Ancaster, Ontario. Precision and accuracy were checked on replicates and against international standards. Electron microprobe analyses were carried out on polished thin sections using the Cameca Superprobe at BGR. The sulfur isotope ratios of pyrite, alunite, and sulphur separates (n=11) were analyzed at Münster University, using a Finnigan Delta E/DeltaPlus mass spectrometer. Sulfide mineral separates were prepared by panning followed by hand picking under a binocular microscope. Sulfur was extracted from sulfide minerals by digestion in $CrCl_2$–HCl and precipitation as Ag_2S, prior to

isotope analysis. The results are reported relative to the Canyon Diablo Troilite. The reproducibility of the results is better than 0.2 ‰.

Vent fluids were collected 750-ml titanium major samplers and with the Hydrothermal Fluid and Particle Sampler (HFPS, Butterfield et al., 2004). Major and trace elements in vent fluids were determined by ion chromatography (Dionex DX500; Cl, Br, SO_4, Na, K, Mg and Ca), flame or graphite furnace atomic absorption (Li, Fe and Mn), ICP-MS with calibration by standard addition and internal standards (Cu, Zn, Al, Rb, Cs and Ba), and ICP-ES (Li, B and Sr) at PMEL. Titration methods were also used for Ca, Mg and Cl, with IAPSO seawater as the standard. For gas analyses, gas-tight titanium samplers were connected directly to a seagoing high vacuum processing line and gases were separated from the fluid fraction by pumping through a trap chilled to -60°C into a calibrated volume. The total gas content was measured manometrically, and then fractions of the dry gas were sealed into glass ampoules for subsequent analysis by mass spectrometry or gas chromatography. More complete details of the analytical methods are provided elsewhere (Butterfield et al., 2004).

References

Bates, R. G., and Culberson, C. H., 1977, Hydrogen ions and the thermodynamic state of marine systems, *in* Anderson, N. R., and Malahoff, A., eds., The Fate of Fossil Fuel CO_2 in the Oceans, Plenum Press, New York, N.Y., United States (USA), p. 45-61.

Butterfield, D. A., Roe, K. K., Lilley, M. D., Huber, J. A., Baross, J. A., Embley, R. W., and Massoth, G. J., 2004, Mixing, reaction and microbial activity in the sub-seafloor revealed by temporal and spatial variation in diffuse flow vents at Axial Volcano: Subseafloor Biosphere at Mid-Ocean Ranges, v. 144, p. 269-289.

Gieskes, J. M., Gamo, T., and Brumsack, H., 1991, Chemical methods for interstitial water analysis aboard Joides Resolution: Ocean Drilling Program, v. Technical Note 15, p. 60.

Lupton, J. E., Weiss, R. F., and Craig, H., 1977, Mantle helium in hydrothermal plumes in the Galapagos Rift: Nature, v. 267, p. 603-604.

Measures, C. I., Yuan, J., and Resing, J. A., 1995, Determination of iron in seawater by flow injection analysis using in-line preconcentration and spectrophotometric detection: Marine Chemistry, v. 50, p. 3-12.

Resing, J. A., Feely, R. A., Massoth, G. J., and Baker, E. T., 1999, The water-column chemical signature after the 1998 eruption of Axial Volcano: Geophysical Research Letters, v. 26, p. 3645-3648.

Resing, J. A., Lupton, J. E., Feely, R. A., and Lilley, M. D., 2004, CO (sub 2) and (super 3) He in hydrothermal plumes; implications for mid-ocean ridge CO (sub 2) flux: Earth and Planetary Science Letters, v. 226, p. 449-464.

Resing, J. A., and Mottl, M. J., 1992, Determination of Manganese in Seawater Using Flow-Injection Analysis with Online Preconcentration and Spectrophotometric Detection: Analytical Chemistry, v. 64, p. 2682-2687.

Table 2. Particulate compositions, Monowai caldera and cone plumes

Location	Sample Name	Total Wt	Vol	Depth	TSM	Na	Mg	Al	Si	P	S Tot	S NV	S V	S V	Cl	K	Ca	Ti
		µg	L	m	µg/L	nM	nM	nM	nM	nM	nM	nM	nM	%	nM	nM	nM	nM
Monowai-caldera	T04D09 R5 N28	688	8.65	1160	79.5	17.13	32.24	49.36	147.71	33.39	1364.57	93.43	1271.1	93.2	1.1	1.1	78.7	2.0
Monowai-caldera	T04D09 R7 N1	475	5.45	1144	87.2	32.17	43.96	77.66	225.69	22.49	1139.74	140.91	998.8	87.6	1.1	2.0	114.4	2.8
Monowai-caldera	T04D09 R9 N17	394	6.25	1039	63.0	29.56	54.41	107.13	314.48	18.59	235.50	113.67	121.8	51.7	1.1	2.4	155.7	3.9
Monowai-caldera	T04D14 R1 N3	385	7.65	1040	50.3	32.32	46.54	90.45	262.27	8.82	45.96	52.37	-6.4	0.0	2.8	2.3	120.4	3.3
Monowai-caldera	T04D14 R5 N17	401	8.45	1141	47.5	25.74	36.55	73.34	212.58	11.31	286.25	79.89	206.4	72.1	1.6	1.6	85.7	2.5
Monowai-caldera	T04D14 R7 N22	440	8.25	1458	53.3	62.55	50.23	92.11	262.18	2.79	19.02	22.69	-3.7	0.0	10.9	3.7	122.7	3.4
Monowai-caldera	V04D12 R1 N15	331	4.35	1072	76.1	34.07	78.53	154.44	454.82	4.83	53.75	62.37	-8.6	0.0	2.7	3.4	215.4	6.1
Monowai-caldera	V04D12 R3 N28	588	6.95	1053	84.6	29.63	67.12	133.09	389.11	12.23	457.40	98.65	358.7	78.4	1.5	2.8	194.5	5.3
Monowai-caldera	V04D12 R5 N26	508	7.25	1034	70.1	25.29	66.23	137.14	393.00	4.23	42.04	45.76	-3.7	0.0	1.6	3.1	195.9	5.4
Monowai-caldera	V04D12 R7 N9	373	8.25	1001	45.2	27.11	48.42	96.73	283.06	3.04	14.87	18.91	-4.0	0.0	1.3	2.0	147.5	3.6
Monowai-caldera	V04D13 R13 N13	792	8.15	1039	97.2	34.20	75.61	151.62	443.14	9.32	25.78	60.75	-35.0	0.0	1.7	3.7	230.1	6.6
Monowai-caldera	V04D13 R5 N17	659	7.85	1186	83.9	30.78	67.66	136.42	395.99	6.23	48.17	53.54	-5.4	0.0	1.7	3.3	196.1	5.5
Monowai-caldera	V04D13 R9 N7	612	7.15	1117	85.6	33.05	66.59	140.69	415.09	10.87	118.23	92.07	26.2	22.1	1.2	3.3	205.3	5.7
Monowai-cone	T04D07 R1 N24	139	8.15	608	17.1	21.48	20.18	37.51	109.19	0.98	bd	3.95	bd	0.0	3.1	0.9	58.0	1.0
Monowai-cone	T04D07 R11 N17	207	8.55	674	24.2	1.53	4.61	bd	17.51	4.96	9.05	19.02	-10.0	0.0	0.9	0.4	130.4	0.1
Monowai-cone	T04D07 R15 N23	219	8.15	134	26.9	14.40	24.66	48.12	142.56	0.86	2.87	13.21	-10.3	0.0	1.0	1.0	86.8	1.5
Monowai-cone	T04D07 R3 N11	145	8.95	455	16.2	14.28	9.26	13.73	46.96	1.36	bd	3.21	bd	0.0	3.0	0.9	53.7	0.4
Monowai-cone	T04D07 R9 N3	301	8.65	809	34.8	28.53	38.14	73.23	213.74	1.15	4.18	14.09	-9.9	0.0	3.2	1.8	103.2	2.5
Monowai-cone	T04D08 R9 N7	1801	7.65	721	235.4	69.32	194.10	403.54	1181.69	2.09	10.39	18.77	-8.4	0.0	1.5	9.9	644.5	20.5
Monowai-cone	V04D07 R1 N22	795	2.35	130	338.3	79.06	35.21	238.99	559.58	11.38	4492.98	480.33	4012.6	89.3	3.5	12.2	180.5	12.7
Monowai-cone	V04D07 R2 N2	1000	1.85	129	540.5	80.98	57.89	318.90	750.60	20.16	5737.46	622.43	5115.0	89.2	4.0	16.8	274.3	22.0
Monowai-cone	V04D14 R1 N22	275	2.45	137	112.2	162.52	35.12	50.86	117.55	49.30	224.47	352.57	-128.1	0.0	28.1	4.9	77.3	4.6
Monowai-cone	V04D14 R5 N26	986	2.25	110	438.2	87.35	46.47	428.78	574.30	107.83	2903.52	1091.28	1812.2	62.4	4.9	15.3	41.0	23.8
Monowai-cone	V04D15 R3 N3	1618	2.25	146	719.1	270.88	100.95	1309.01	1136.49	94.91	5641.12	1289.69	4351.4	77.1	24.2	29.3	175.4	35.4
Monowai-cone	V04D15 R5 N15	8049	6.45	133	1247.9	60.98	48.16	1960.19	776.21	96.36	8138.65	3651.65	4487.0	55.1	12.1	22.5	160.2	39.0
Monowai-cone	V04D15 R8 N28	10713	4.15	117	2581.4	0.00	0.00	0.00	0.00	0.00	19372.60	0.00	19372.6	100.0	11.3	49.8	304.2	74.2
Monowai-cone	V04D16 R5 N26	3729	6.65	625	560.8	103.64	224.17	518.55	1426.45	3.37	41.23	86.81	-45.6	0.0	1.7	12.4	679.0	21.8

bd = below detection; TSM = total suspended material; S NV = non-volatile sulfur; S V = volatile S

Table 2. Particulate compositions, Mon

Location	Sample Name	V	Cr	Mn	Fe	Ni	Cu	Zn	As	Rb	Sr	Ba	W	Pb	Bi
		nM	nM	nM	nM	nM	nM	nM	nM	nM	nM	nM	nM	nM	nM
Monowai-caldera	T04D09 R5 N28	0.47	0.15	0.77	139.1	0.09	0.41	0.77	0.27	bd	0.27	0.66	0.048	0.043	bd
Monowai-caldera	T04D09 R7 N1	0.42	0.09	1.33	118.5	0.13	1.06	3.88	0.22	bd	0.27	0.61	bd	0.057	bd
Monowai-caldera	T04D09 R9 N17	0.45	0.09	2.29	121.7	0.09	0.43	0.77	0.15	bd	0.31	0.71	0.054	0.057	0.026
Monowai-caldera	T04D14 R1 N3	0.31	0.06	1.71	84.9	0.29	0.23	0.24	0.05	bd	0.21	0.47	0.016	0.028	bd
Monowai-caldera	T04D14 R5 N17	0.30	0.05	1.49	77.2	0.27	0.65	0.70	0.08	bd	0.17	0.45	0.019	0.025	bd
Monowai-caldera	T04D14 R7 N22	0.27	0.06	2.23	69.3	0.27	0.15	0.28	bd	bd	0.19	0.43	bd	0.015	bd
Monowai-caldera	V04D12 R1 N15	0.49	0.09	2.76	129.9	0.47	0.28	0.21	0.04	bd	0.39	0.73	0.050	bd	bd
Monowai-caldera	V04D12 R3 N28	0.49	0.12	2.28	137.1	0.34	0.35	0.24	0.09	bd	0.39	0.74	0.032	0.039	bd
Monowai-caldera	V04D12 R5 N26	0.39	0.10	2.31	111.6	0.32	0.50	0.61	0.05	bd	0.38	0.64	0.039	0.024	bd
Monowai-caldera	V04D12 R7 N9	0.28	0.05	1.71	75.2	0.27	0.16	0.15	bd	bd	0.28	0.47	bd	0.008	bd
Monowai-caldera	V04D13 R13 N13	0.62	0.10	3.09	156.8	0.04	0.40	0.32	0.06	bd	0.41	0.84	0.034	0.029	bd
Monowai-caldera	V04D13 R5 N17	0.44	0.07	2.93	122.6	0.30	0.68	0.25	0.05	bd	0.31	0.62	0.036	0.024	bd
Monowai-caldera	V04D13 R9 N7	0.53	0.09	2.89	141.3	0.32	0.45	0.40	0.08	bd	0.35	0.74	bd	0.022	bd
Monowai-cone	T04D07 R1 N24	0.08	0.02	0.47	19.9	0.10	0.16	0.15	bd	bd	0.18	0.24	0.033	0.018	0.022
Monowai-cone	T04D07 R11 N17	0.01	0.01	0.12	1.7	0.10	0.02	0.05	bd	bd	0.73	0.06	0.020	0.013	bd
Monowai-cone	T04D07 R15 N23	0.12	0.02	0.64	29.0	0.10	0.13	0.08	bd	bd	0.24	0.28	0.029	0.010	bd
Monowai-cone	T04D07 R3 N11	0.05	0.01	0.29	8.2	0.10	0.03	0.19	bd	bd	0.32	0.20	0.026	0.021	bd
Monowai-cone	T04D07 R9 N3	0.18	0.05	0.97	47.4	0.11	0.27	0.25	bd	bd	0.19	0.35	0.036	0.016	bd
Monowai-cone	T04D08 R9 N7	1.57	0.28	7.90	427.5	0.15	0.76	0.41	0.02	bd	0.79	1.88	0.050	0.009	bd
Monowai-cone	V04D07 R1 N22	0.67	0.35	1.28	108.9	0.31	0.55	0.72	0.10	bd	1.44	0.71	bd	0.042	0.079
Monowai-cone	V04D07 R2 N2	1.32	1.17	2.67	230.3	0.42	1.33	2.31	0.20	bd	2.06	1.93	0.107	0.386	bd
Monowai-cone	V04D14 R1 N22	1.94	1.01	0.65	284.9	bd	0.48	0.81	0.78	bd	0.55	2.51	0.104	0.081	bd
Monowai-cone	V04D14 R5 N26	8.32	2.14	0.84	1063.6	0.09	1.20	0.64	4.07	bd	1.15	bd	0.158	0.142	bd
Monowai-cone	V04D15 R3 N3	8.38	2.30	2.10	1177.5	bd	1.17	0.69	4.60	bd	2.20	bd	0.227	0.106	bd
Monowai-cone	V04D15 R5 N15	8.42	2.56	1.83	1368.9	bd	1.76	2.33	6.21	bd	2.94	10.59	0.341	0.141	0.049
Monowai-cone	V04D15 R8 N28	14.68	2.81	4.36	2607.6	bd	2.28	3.30	11.25	bd	6.38	18.84	0.647	0.153	0.109
Monowai-cone	V04D16 R5 N26	1.60	0.29	7.73	445.7	0.09	1.02	0.53	0.04	bd	0.84	1.93	0.035	0.020	0.030

bd = below detection; TSM = total sus

Table 3. Composition of volcanic glass, least-altered, and mineralized basalts and basaltic andesites, and alteration crusts and native sulphur precipitates from the Mussel Ridge, Monowai caldera, northern Kermadec island arc, SW-Pacific.

		Basalt-andesite Glass n=7	Basalt-andesite least-altered n=15	Basalt-andesite mineralized n=21	Alteration crust n=5	Native sulfur n=3
SiO_2	wt.%	55.85	51.72	55.09	50.32	0.62
TiO_2	wt.%	1.01	0.95	1.03	1.17	0.01
Al_2O_3	wt.%	14.72	14.32	15.08	16.55	0.18
Fe_2O_3	wt.%	12.24	8.34	9.87	6.53	0.13
MnO	wt.%	0.23	0.10	0.12	0.07	0.00
MgO	wt.%	3.36	2.44	2.72	1.91	0.16
CaO	wt.%	7.85	4.91	5.25	3.59	0.14
Na_2O	wt.%	3.20	3.07	4.36	3.41	0.31
K_2O	wt.%	0.54	0.41	0.40	0.48	0.09
P_2O_5	wt.%	0.15	0.11	0.10	0.14	0.01
S	wt.%	0.28	2.25	1.39	0.57	98.33
Cl	wt.%	0.08	0.02	0.03	0.01	bl
LOI	wt.%	0.43	10.48	5.35	15.02	
Total	wt.%	99.81	99.77	99.86	99.72	99.96
Au	ppb	bl	bl	69	n.d.	n.d.
Ag	ppm	bl	bl	bl	n.d.	n.d.
As	ppm	6.8	10	22	11	4.5
Ba	ppm	158	167	165	169	9.0
Bi	ppm	n.d.	1.2	0.30	bl	n.d.
Co	ppm	30	26	30	21	bl
Cr	ppm	8	20	12	5.3	6.5
Cs	ppm	3.6	5.0	3.8	4.5	bl
Cu	ppm	103	94	140	67	11
Ga	ppm	18	15	16	12	bl
Ge	ppm	1.4	0.14	0.75	n.d.	n.d.
Hf	ppm	5.0	3.5	2.1	8.0	bl
Mo	ppm	3.0	9.4	19	9.2	5.0
Nb	ppm	3.6	bl	3.7	3.0	bl
Ni	ppm	7.7	8.5	14	6.3	4.3
Pb	ppm	5.5	7.0	13	4.5	4.5
Rb	ppm	8.9	6.0	5.6	4.8	5.0
Sb	ppm	0.19	0.75	5.3	bl	bl
Sc	ppm	35	30	32	29	1.0
Sn	ppm	bl	3.8	4.4	bl	bl
Sr	ppm	208	384	287	605	6.7
Ta	ppm	3.6	bl	5.0	bl	bl
Th	ppm	0.34	4.0	3.1	4.3	3.0
Tl	ppm	0.08	0.30	0.12	n.d.	n.d.
U	ppm	0.27	4.3	1.0	bl	bl
V	ppm	265	242	259	252	5.5
Y	ppm	28	16	18	14.6	bl

Zn	ppm	110	52	62	31.6	6.0
Zr	ppm	66	58	66	68.4	9.0
La	ppm	3.5	3.8	3.1	n.d.	n.d.
Ce	ppm	10.4	9.5	9.3	n.d.	n.d.
Pr	ppm	1.7	n.d.	1.7	n.d.	n.d.
Nd	ppm	9.0	13	9.7	n.d.	n.d.
Sm	ppm	3.0	1.4	2.0	n.d.	n.d.
Eu	ppm	1.1	0.97	1.21	n.d.	n.d.
Gd	ppm	4.1	n.d.	4.1	n.d.	n.d.
Tb	ppm	0.77	n.d.	0.79	n.d.	n.d.
Dy	ppm	4.9	n.d.	5.2	n.d.	n.d.
Ho	ppm	1.0	n.d.	1.1	n.d.	n.d.
Er	ppm	3.0	n.d.	3.3	n.d.	n.d.
Tm	ppm	0.47	n.d.	0.49	n.d.	n.d.
Yb	ppm	3.2	2.2	2.6	n.d.	n.d.
Lu	ppm	0.47	0.35	0.41	n.d.	n.d.

n.d. = not determined; bd = below detection.

Table 4. $\delta^{34}S$ values for different sulfur minerals and species in altered basaltic andesites from Mussel Ridge, showing heavier S isotopes in alunite separates and extremely light S isotopes for pyrite concentrates. The isotopic values of native S are close to the magmatic $\delta^{34}S$ signature for island arc volcanics. Therefore, native S in Monowai samples may have formed by direct condensation of magmatic SO_2.

Sample	Pyrite [‰]		Alunite [‰]		Native Sulfur [‰]	
26 TVG x	-8.2	-8.5	+1.9	+1.2		
26 TVG s			+2.2			
26 TVG 01			+11.1	+11.3		
27TVG02A					+2.8	+2.5
27TVG02B					+1.9	+1.2

Table 5. Composition of vent fluids and ambient seawater, Mussel Ridge, Monowai caldera (*Pisces V*)

Sample	Dive	Type	Date	Vent Abbr.	Long dec deg W	Lat dec deg S	Depth (m)	T (ºC)	pH	Si µmol/kg	H_2S µmol/kg	SO_4 mM/kg	Cl titr mM/kg	Mg-titr. mM/kg	Ca-titr. mM/kg	Na mM/kg	K mM/kg	Fe µmol/kg	Mn µmol/kg	Fe/Mn mol/mol
HFS 18 f/bag	614	HFS	9-Apr-05	MCa10b	177.168317	25.804113	1141	52	5.47	1431	3537	26.31	517.24	48.30	11.47	431.0	9.42	0.4	163.4	0.002
HFS 16 f/bag	614	HFS	9-Apr-05	MCa10b	177.168317	25.804113	1141	52	5.41	1431	4017	26.16	515.31	48.07	11.43	424.5	9.27	0.4	168.0	0.002
HFS 19 bag	614	HFS	9-Apr-05	MCa10b	177.168317	25.804113	1141	52	5.39	1470	3869	26.24	517.79	48.30	11.47	424.7	9.28	4.5	165.9	0.027
HFS 8 bag	614	HFS	9-Apr-05	MCa8	177.167917	25.803958	1166	44	5.64	983	3169	26.34	518.62	49.30	11.03	433.0	9.44	0.6	96.5	0.006
HFS 11 f/bag	614	HFS	9-Apr-05	MCa8	177.167917	25.803958	1166	43	5.53	1032	3306	26.68	518.55	49.22	11.02	441.9	9.71	0.4	102.5	0.004
HFS 6 piston	614	HFS	9-Apr-05	MCa8	177.167917	25.803958	1166	35	5.72	833	2590	27.18	527.40	49.89	10.93	441.0	9.61	0.5	75.3	0.007
MS Blue	613	MS	8-Apr-05	MCa2	177.167795	25.803762	1171	56	6.20	537	684	27.52	539.27	51.42	11.12	459.3	10.00	0.8	not analyzed	
HFS 14 f/bag	614	HFS	9-Apr-05	MCa9	177.167773	25.803996	1157	26	5.88	886	769	26.78	538.20	50.44	12.17	425.6	9.30	70.5	256.3	0.275
HFS 20 piston	614	HFS	9-Apr-05	MCa9	177.167773	25.803996	1157	32	5.79	974	1363	26.78	538.13	50.40	12.12	450.3	9.86	0.3	417.1	0.001
HFS 1 f/piston	614	HFS	9-Apr-05	MCa10	177.168283	25.804156	1143	6	7.00	118	1	27.77	537	52.08	10.40	430.4	9.25	0.4	25.2	0.016
HFS 5 piston	614	HFS	9-Apr-05	MCa10	177.168283	25.804156	1143	9	6.65	230	130	27.89	538.07	52.06	10.72	441.4	9.61	0.4	61.5	0.007
HFS 22 piston	614	HFS	9-Apr-05	MCa11	177.168973	25.804837	1079	25	5.77	925	1054	26.68	541.29	50.21	12.44	385.9	8.41	2.3	371.0	0.006
MS Blue	615	MS	10-Apr-05	MCa12	177.169449	25.805783	1025	13	6.21	408	685	28.35	536.52	52.13	11.15	455.8	9.91	5.2	30.9	0.168
MS White	612	MS	7-Apr-05	AmbSW	177.168579	25.806963	1052	3	7.68	57	0	28.13	540	52.33	10.21	457.7	9.97	1.3	0.6	2.167